Measuring Conflict in Multi-Objective Optimization: A Case Study of the Impact of Climate Change on the Joint Provision of Forest Ecosystem Services

Nicholas D. C. Kullman

A thesis
submitted in partial fulfillment of the
requirements for the degree of

Master of Science

University of Washington

2016

Committee:

Sándor F. Tóth, Chair

David Butman

W. Art Chaovalitwongse

Program Authorized to Offer Degree:
Quantitative Ecology and Resource Management

University of Washington

Abstract

Measuring Conflict in Multi-Objective Optimization:
A Case Study of the Impact of Climate Change on
the Joint Provision of Forest Ecosystem Services

Nicholas D. C. Kullman

Chair of the Supervisory Committee:
Associate Professor Sándor F. Tóth
School of Environmental and Forest Sciences

DRAFT

Forests provide a bounty to humans through ecosystem services such as wildlife habitat, recreation, and water and air purification. Forest managers seek to maximize the provision of ecosystem services and often do so for multiple ecosystem services simultaneously. While many studies predict that climate change will impact forests' ability to provide ecosystem services, no research has addressed the question of how climate change will impact the joint provision of ecosystem services. I address this question here in an attempt to better understand how the relationships between ecosystem services will change with climate. For example, how much additional fire hazard must be assumed in order to maintain an amount of habitat for a particular species. To study this question, I consider the growth of a forested area in the Deschutes National Forest under three climate scenarios of varying intensity. This area provides three competing ecosystem services whose joint provision is assessed under each of the climate scenarios: northern spotted owl habitat, water quality, and resistance to wildfire.

I find that ...

TABLE OF CONTENTS

LIST OF FIGURES

LIST OF TABLES

ACKNOWLEDGMENTS

DRAFT

Thank you to all who contributed to my earning this degree.

DEDICATION

To Rachel, my parents and grandparents

Chapter 1

MEASURING CONFLICT IN MULTI-OBJECTIVE OPTIMIZATION: A CASE STUDY OF THE IMPACT OF CLIMATE CHANGE ON THE JOINT PROVISION OF FOREST ECOSYSTEM SERVICES

1.1 Introduction

Many tasks in resource allocation are multi-objective. The design of aircraft involves balancing cost and efficiency [80]. Hospitals seek to manage personnel and equipment in order to maximize patient throughput while minimizing cost and required back-up [39]. Food production balances processing time with nutrient retention [69]. Forest managers aim to provide carbon sequestration and wildlife habitat while also maximizing timber revenues [76].

Given a set of solutions to one of these resource allocation problems, a decision maker chooses one to enact. Often, no one solution simultaneously optimizes all objectives, and the decision maker must therefore choose a solution that represents a preferred compromise among them. In such cases, there is some amount of conflict among the objectives. This is in contrast to compatible or harmonious objective relationships in which the objectives improve simultaneously.

In the case of aircraft design, cost and efficiency conflict with one another, since more efficient design details tend to cost more. Similarly, hospitals may increase patient throughput by increasing the number of doctors available, but this decision would increase costs. Food production engineers can maximize nutrient retention by reducing the temperature at which processing occurs, but this would lengthen the time required to reach acceptable microbiological levels. Forest managers can maximize timber revenue by removing large old-growth timber, but this would reduce the available wildlife habitat.

While the preferred solution may vary by decision maker, a rational decision maker will prefer one which is Pareto efficient; that is, a solution in which no objective can be improved without compromising another. Multi-objective optimization affords the knowledge of such solutions and can help guide the decision maker by revealing where objectives can be achieved simultaneously and where they conflict. Having access to the set of Pareto efficient solutions may also help the decision maker locate solutions where compromises in one objective allow outweighing improvements in another. For instance the forest manager may discover that forgoing small amounts of timber revenues allows for the sequestration of significantly more carbon. Or the hospital may be able to increase patient throughput substantially if they hire one additional oncologist. Regardless of whether a decision maker selects a solution providing such gains, the awareness of these relationships enables more informed decision making.

In addition to studying conflict within a system, we may further study it at the super-system level. Consider the situation in which a decision maker oversees multiple systems, each with its own set of Pareto efficient solutions. This could be the case for a manager overseeing multiple hospitals or multiple food processing facilities. Alternatively, each system may correspond to a different regulatory or environmental scenario, such as a forest manager analyzing resource allocation under various realizations of climate change. In such instances, understanding the differences in the conflict relationships between systems may benefit the decision maker, allowing them to ask questions such as: How does the relationship between carbon sequestration and timber revenues vary under different climate change scenarios? Do all hospitals require the same increase in staffing costs to improve patient throughput?

To date, the multi-objective optimization literature has not addressed conflict at the super-system level. We do so for the first time here, laying a foundation for quantitative conflict analysis. To perform this investigation, we draw on Pareto set indicators and correlation measures commonly used in the field of evolutionary multi-objective optimization (EMO). In EMO, the Pareto set indicators are generally used to assess the performance of algorithms that approximate the Pareto set [86], and the correlation measures are used as

an aid to increase the computational tractability of the problems encountered in EMO [10].

Here we adapt these measures for real-world application, using them to study conflicting management objectives across systems. To further our insight into the origin of conflict within a system, we also propose a new metric for quantifying the conflict between pairs of objectives. The new pairwise conflict metric developed here improves on other commonly used pairwise conflict metrics such as the Pearson and Spearman coefficients. Unlike any current metric, the one we propose simultaneously captures mutual objective achievement and accurately identifies the absence of conflict between objectives. We demonstrate the novel utility of the existing and proposed conflict metrics on a multi-objective scenario-based case study in the Deschutes National Forest.

In the upcoming sections, we define terminology and the measures of conflict. Then we describe the case study and present its results, including the application of the new and existing conflict metrics. We conclude with discussion, summary, and suggestions for future research.

1.2 Methods

We lay a foundation for quantitative conflict analysis of multi-objective systems. The analysis centers on the use of three metrics: two existing measures from EMO and one that we have developed and introduce for the first time here. A case study on the impacts of climate change on forest management serves to illustrate the conflict analysis. Prior to describing the case study, we first define terminology and describe each of the measures used in our analysis.

1.2.1 Terminology

The multi-objective problem Consider the M-objective optimization problem

Maximize

$$\mathbf{f} = [f_1(\mathbf{x}), f_2(\mathbf{x}), \ldots, f_M(\mathbf{x})] \tag{1.1}$$

subject to

$$\mathbf{x} \in X \tag{1.2}$$

with *objective functions* $f_i(\mathbf{x}), i \in \{1, \ldots, M\}$ and feasible *decision vectors* (or *solutions*) $\mathbf{x} \in \mathbb{R}^n$ where n is the number of decision variables in the optimization problem. A set of equality and inequality constraints determine the *feasible decision space* X. Solutions in X are referenced by superscripts: $X = \{\mathbf{x}^1, \mathbf{x}^2, \ldots, \mathbf{x}^{|X|}\}$. Each objective function $f_i : \mathbb{R}^n \mapsto \mathbb{R}$ maps decision vectors to scalars in $\mathbb{R}$. The vector objective function $\mathbf{f} : X \mapsto \mathbb{R}^M$ maps the feasible decision space to the *objective space* $\mathbb{R}^M$. The set of all objective functions is the *objective set* $\mathcal{M} = \{f_1, \ldots, f_M\}$.

Dominance and frontiers A solution $\mathbf{x}^1$ is said to *dominate* another solution $\mathbf{x}^2$ ($\mathbf{x}^1 \succ \mathbf{x}^2$) if

$$\exists f_i \in \mathcal{M} : f_i(\mathbf{x}^1) > f_i(\mathbf{x}^2) \text{ and } \forall f_i \in \mathcal{M}\ f_i(\mathbf{x}^1) \geq f_i(\mathbf{x}^2) \tag{1.3}$$

A solution $\mathbf{x}^1 \in X$ is *non-dominated* if

$$\nexists \mathbf{x}^2 \in X : \mathbf{x}^2 \succ \mathbf{x}^1 \tag{1.4}$$

For a rational decision maker, all dominated solutions may be removed from the analysis, since for a dominated solution $\mathbf{x}^2$ there exists another solution $\mathbf{x}^1$ which is better: $\mathbf{x}^1$ achieves more in at least one objective than $\mathbf{x}^2$, and $\mathbf{x}^1$ does not achieve less in any objective than $\mathbf{x}^2$. Thus, the decision maker will always select a solution from the set of non-dominated decision vectors that solve the multi-objective problem (1.1) and (1.2). We refer to this set as the *Pareto-optimal set* $P = \{\mathbf{x} \in X | \nexists \mathbf{y} \in X : \mathbf{y} \succ \mathbf{x}\}$.

The *Pareto-optimal frontier*, the *efficient frontier* or, simply, the *frontier* Z is the corresponding set of M-dimensional *objective vectors* $\mathbf{z} = [f_1(\mathbf{x}), f_2(\mathbf{x}), \ldots, f_M(\mathbf{x})]$. That is,

$$Z = \{\mathbf{z} = [f_1(\mathbf{x}), \ldots, f_M(\mathbf{x})] \mid \mathbf{x} \in P\} \tag{1.5}$$

Objective vectors' components are referred to in subscripts:

$$\mathbf{z} = [z_1, z_2, \ldots, z_M] \tag{1.6}$$

Objective vectors provide the decision maker with knowledge of the objective achievement of a solution $\mathbf{x}$ - the ith component of an objective vector $\mathbf{z}$ represents the achievement in objective i by the corresponding decision vector $\mathbf{x}$.

Ideal and nadir objective vectors The *ideal objective vector* is defined as the vector

$$\mathbf{z}^{\text{ideal}} = \max_{\mathbf{x} \in X} \{f_i(\mathbf{x})\} \quad \forall i \in \mathcal{M}. \tag{1.7}$$

Analogously, define the nadir solution as the vector

$$\mathbf{z}^{\text{nadir}} = \min_{\mathbf{x} \in X} \{f_i(\mathbf{x})\} \quad \forall i \in \mathcal{M}. \tag{1.8}$$

The ideal objective vector represents the impossible ideal scenario in which each objective is simultaneously optimized. The nadir objective vector represents the worst case scenario in which each objective attains its lowest value. These solutions are the diagonal corners of the minimum bounding box for the efficient frontier Z. Since they provide upper and lower bounds for each objective, they serve as reference points against which the decision maker can compare solutions.

Trade-offs The *trade-off* between two objective vectors $\mathbf{z}^1$ and $\mathbf{z}^2$ is the vector of differences in their objective achievements:

$$\tau^{1,2} = [z_1^2 - z_1^1, z_2^2 - z_2^1, \ldots, z_M^2 - z_M^1] \tag{1.9}$$

The components of $\tau^{1,2}$ represent the amount of each objective that would be sacrificed or gained by selecting $\mathbf{z}^2$ instead of $\mathbf{z}^1$. Note that $\tau^{1,2} = -\tau^{2,1}$.

Sub-dimensions During analysis, we often wish to consider only a subset of the objectives $\mathcal{L} \subset \mathcal{M}$. We define such subsets as *sub-dimensional objective sets*. In these cases, it is simpler to work with constructs that have only those components that correspond to the objectives in $\mathcal{L}$. For instance, define the *sub-dimensional objective vector* for the solution $\mathbf{x}^i$ as $\mathbf{z}^i_{\mathcal{L}}$ which has components $\forall \ell \in \mathcal{L}. z^i_\ell = f_\ell(\mathbf{x}^i)$. Define the *sub-dimensional trade-off* $\tau^{1,2}_{\mathcal{L}}$ as the vector with components $\forall \ell \in \mathcal{L}. \tau^{1,2}_\ell$.

Relative objective achievements, relative objective vectors, and relative trade-offs Using the nadir and ideal objective vectors, we can represent each solution as a vector of its relative objective achievements. This allows for dimensionless and scale-agnostic comparison of solutions. For an objective vector $\mathbf{z}$, its *relative achievement in objective* i is

$$\overline{z_i} = \frac{z_i - z_i^{\text{nadir}}}{z_i^{\text{ideal}} - z_i^{\text{nadir}}}, \tag{1.10}$$

and the corresponding *relative objective vector* is

$$\bar{\mathbf{z}} = [\overline{z_1}, \overline{z_2}, \ldots, \overline{z_M}]. \tag{1.11}$$

For two objective vectors $\mathbf{z}^1$ and $\mathbf{z}^2$, the corresponding *relative trade-off* is

$$\bar{\tau}^{1,2} = \left[\overline{z_1^2} - \overline{z_1^1}, \overline{z_2^2} - \overline{z_2^1}, \ldots, \overline{z_M^2} - \overline{z_M^1}\right] \tag{1.12}$$

Conflict, monotonicity, bundles and stacks We use the following test to determine if Objectives in an objective set $\mathcal{L}$ *do not conflict* if the objectives improve simultaneously: $\forall \mathbf{z}^1, \mathbf{z}^2 \in Z, i \in \mathcal{L}$

$$(z_i^1 \geq z_i^2) \Rightarrow (z_j^1 \geq z_j^2) \quad \forall j \in \mathcal{L}, j \neq i \tag{1.13}$$

If (1.13) does not hold, then the objectives conflict. Any pair of objectives $i, j \in \mathcal{M}$ such that equation (1.13) holds are said to *increase monotonically*. In the case of monotonically increasing objectives i and j, improving objective i also yields improvement in objective j. Conversely, if

$$(z_i^1 \geq z_i^2) \Rightarrow (z_j^1 \leq z_j^2) \quad \forall \mathbf{z}^1, \mathbf{z}^2 \in Z, j \neq i \tag{1.14}$$

holds, then objectives i and j are said to *decrease monotonically*.

When the objectives represent goods or services, a set of objectives that conflict is defined as a *bundle* and a set of objectives that do not conflict is defined as a *stack*.

Equation (1.13) checks for monotonically increasing relationships among objectives. This means of detecting conflict is functionally equivalent to that used by many studies, such as Brockhoff and Zitzler (2009) [11] and Purshouse and Fleming (2003) [61].

1.2.2 Measuring conflict: the hypervolume indicators

Any multi-objective problem whose efficient frontier consists of more than one solution contains conflict. The decision maker responsible for these multi-objective systems must determine which solution represents the best compromise among the objectives, and their ability to do so is improved by knowledge of the conflict in the system. This includes both the amount of overall system conflict as well as the source of that conflict. For the former, we can draw on existing measures from EMO; for the latter, we propose a new metric that quantifies the conflict between pairs of objectives. We begin with a description of the measures from EMO that we use to measure system-level conflict: the hypervolume indicators.

Hypervolume indicator

The *hypervolume indicator* $I_{H1}(Z)$ measures the percentage of the objective space that is bounded by the non-dominated objective vectors $\mathbf{z} \in Z$. See Figure 1.1. Systems with less conflict will produce solutions with greater joint provision of objectives, leading to a greater proportion of enclosed objective space and thus a larger value for the hypervolume. In contrast, systems with more conflict produce solutions with less joint provision of objectives, leading to a lesser proportion of enclosed objective space and a smaller value for the hypervolume. That is, the greater the value of the hypervolume indicator, the lower the conflict in the system.

To measure the hypervolume indicator, for each relative objective vector $\overline{\mathbf{z}^i}$ in the frontier Z, define its corresponding hyperrectangle r_i. r_i is the M-orthotope with the pair of

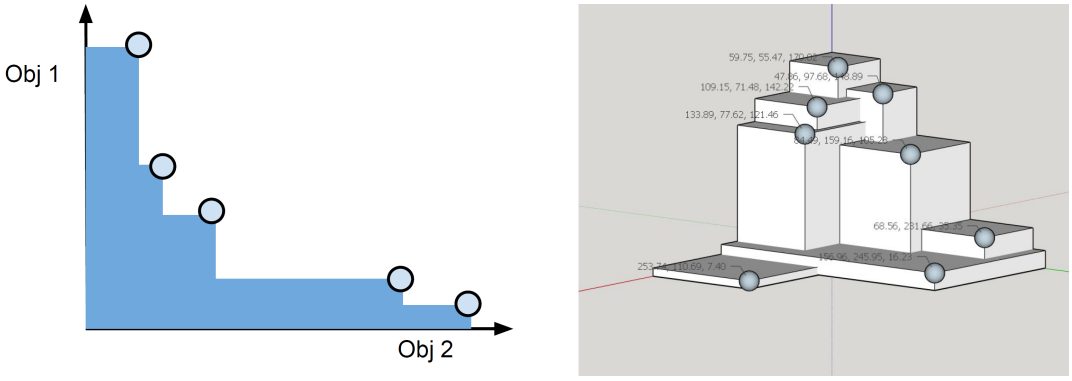

Figure 1.1: Depiction of the hypervolumes of frontiers with two objectives (left) and three objectives (right).

diagonally opposite points the origin and the point defined by the components of the relative objective vector $\overline{\mathbf{z}}^i$. Then the hypervolume indicator is the volume of the union of these hyperrectangles:

$$I_{H1}(Z) = \text{vol}\left(\bigcup_{i=1}^{|Z|} r_i\right). \tag{1.15}$$

Given two frontiers Z^1 and Z^2, how do you interpret a difference in their hypervolumes? Consider Figure 1.2 which shows the relative objective space for a two-dimensional frontier. The shaded square in the lower left represents an achievement of 10% in each objective. Since the objective space of the relative objective vectors is bounded by the 1×1 square, this corresponds to 1% of the objective space. So if Z^1 and Z^2 are bi-objective frontiers ($M = 2$) and if $I_{H1}(Z^1) - I_{H1}(Z^2) = 0.01$, then the solutions in frontier Z^1 bound an area equivalent to an additional 10% achievement in each objective beyond that bounded by the solutions in Z^2. Small differences in the values of the hypervolume represent significant objective gains.

In general, an increase of h in the value of the hypervolume equates to an increase in each objective of $h^{1/M}$. So if Z^1 and Z^2 were tri-objective ($M = 3$) then an improvement of .01 in the value of the hypervolume would represent an improvement of about 22% in each

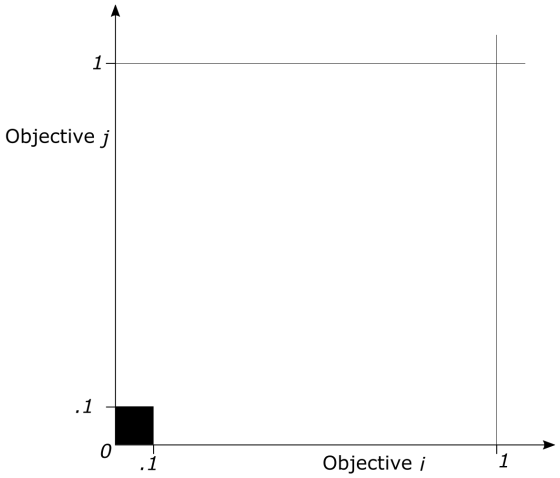

Figure 1.2: To compute the hypervolume, we use the relative objective vectors for the solutions in a frontier. As a result, the frontier is bounded by the M-cube which has a pair of diagonal corners at the origin and $\vec{1}$. Shown here is the 2-cube (a square) representing the space in which we compute the hypervolume for a bi-objective frontier ($M = 2$). The space bound by the shaded square in the lower left represents an achievement of 10% in each objective yet makes up only 1% of the objective space. Its intent is to show that small differences in hypervolumes are significant: with two objectives, an improvement of 0.01 in the value of the hypervolume represents an additional achievement of 10% in each objective.

objective.

Binary Hypervolume Indicator

If a frontier Z^2 is found to have a smaller hypervolume than another Z^1, one may wonder whether Z^2 is completely enclosed within Z^1 or simply bounds a different but smaller region of the relative objective space. We use the binary hypervolume indicator to address this question. The binary hypervolume $I_{H2}(Z^1, Z^2)$ computes the volume of the objective space bounded by Z^1 but not by Z^2. See Figure 1.3. As such, if Z^2 is completely enclosed within Z^1, then $I_{H2}(Z^2, Z^1) \leq 0$. On the other hand, if $I_{H2}(Z^2, Z^1) > 0$ then Z^2 encloses regions of the objective space that Z^1 does not.

Following the definition proposed by Zitzler (1999) [85], the *binary hypervolume indicator*

of two frontiers Z^1 and Z^2 is [85]

$$I_{H2}(Z^1, Z^2) = I_{H1}(Z^1 + Z^2) - I_{H1}(Z^2) \tag{1.16}$$

where $I_{H1}(Z^1 + Z^2)$ is the unary hypervolume indicator of the frontier that consists of the nondominated points in $\{Z^1 \cup Z^2\}$. See the lower-left panel in Figure 1.3.

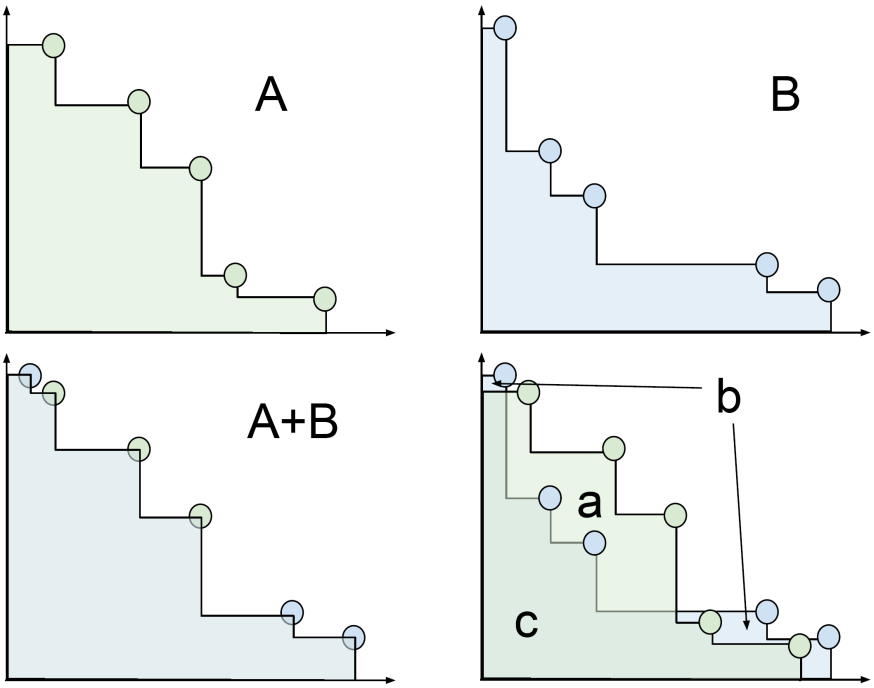

Figure 1.3: Depiction of the binary hypervolume indicator. The individual frontiers are shown in the top row: frontier A (left) and frontier B (right). The merged frontier $A + B$ is shown in bottom left - note the absence of points that were dominated when combined. Following the naming of regions as shown in the bottom right figure, the binary hypervolume indicator is equal to

$$I_{H2}(A, B) = (\text{area}_a + \text{area}_b + \text{area}_c) - (\text{area}_b + \text{area}_c) = \text{area}_a$$

1.2.3 Computing the hypervolume indicator

Computing the hypervolume is a nontrivial task that has received attention from the EMO community. For a comparison of previous algorithms that compute the hypervolume, see

While (2006) [81]. For this work, we developed our own algorithm to compute the hypervolume indicator.

The algorithm begins with a list of the relative objective vectors, denoted in the algorithm simply by $\mathbf{z} \in Z$. These vectors are assumed to be sorted in descending order based on their mth component, for some arbitrary objective $m \in \mathcal{M}$. We define the sub-dimensional objective set $\mathcal{L} = \mathcal{M} \backslash \{m\}$ whose cardinality we denote by $|\mathcal{L}| = L = M - 1$.

We initialize the algorithm with an empty set of non-dominated solutions in L dimensions; refer to this set as G. Let the volume of this nondominated set be denoted $\overline{V}$. We sequentially add solutions from Z to G, at each iteration adding the contribution of the solution $\mathbf{z}$ to the hypervolume indicator V. These contributions are computed by multiplying the solution's mth component z_m by its contribution to the volume of G, $\overline{V}_{\mathbf{z}}$. See Figure 1.5 for a visual reference (the solutions' contribution to the volume of G, $\overline{V}_{\mathbf{z}}$, are the yellow regions in the figure).

$\overline{V}_{\mathbf{z}}$ is computed as follows. Initialize $\overline{V}_{\mathbf{z}} = 0$, and add $\mathbf{z}$ to the set G. Remove from G any solutions that are dominated by $\mathbf{z}$ in L dimensions. Add to $\overline{V}_{\mathbf{z}}$ the value of the volume of $\mathbf{z}$ in L dimensions (the union of the yellow and gray areas in Figure 1.5); this is simply the product of its components z_ℓ for $\ell \in \mathcal{L}$. Then subtract from $\overline{V}_{\mathbf{z}}$ the volume of G prior to the addition of $\mathbf{z}$ (the union of the gray and white areas in Figure 1.5). The last step is to compute and add back in the volume of the "sides" of G that were subtracted in the previous step (the white areas in Figure 1.5). This volume is computed by taking the sum over each dimension $\ell \in \mathcal{L}$ of the areas along that dimension enclosed by the existing solutions in G. Pseudocode for this algorithm is presented in Figure 1.4.

Figure 1.4: Algorithm to compute the hypervolume V of a Pareto frontier. Prior to running the algorithm, pick an objective m from the objective set $\mathcal{M}$ and define the sub-dimensional objective set $\mathcal{L} = \mathcal{M} \backslash \{m\}$. Then sort $\mathbf{z} \in Z$ in descending order by their mth component. Here, $\mathbf{z} \in Z$ is the set of relative objective vectors. Let $\overline{V}_{\mathbf{z}}$ be the $(M-1)$-dimensional volume contribution of the solution $\mathbf{z}$, and let $\mathbf{g} \in G$ be the non-dominated objective vectors in $M-1$ dimensions.

$V \leftarrow 0$
$\overline{V} \leftarrow 0$
$G \leftarrow \emptyset$
for all $\mathbf{z} \in Z$ **do**
    $\overline{V}_{\mathbf{z}} \leftarrow \prod_{\ell \in \mathcal{L}} z_\ell - \overline{V}$
    for all $\mathbf{g} \in G$ **do**
        if $g_\ell < z_\ell \, \forall \ell \in \mathcal{L}$ **then**
            $G \leftarrow G \backslash \{\mathbf{g}\}$
        end if
    end for
    for all $\ell \in \mathcal{L}$ **do**
        $G_{\mathbf{z},\ell} := \{ \mathbf{g} \in G : g_\ell > z_\ell \}$
        Sort $\mathbf{g} \in G_{\mathbf{z},\ell}$ in ascending order by ℓth component, g_ℓ
        $v_i \leftarrow z_\ell$
        for all $\mathbf{g} \in G_{\mathbf{z},\ell}$ **do**
            $v_t \leftarrow g_\ell$
            $\delta_\ell := v_t - v_i$
            $\overline{V}_{\mathbf{z}} \leftarrow \overline{V}_{\mathbf{z}} + \delta_\ell \prod_{\lambda \in \mathcal{L} \backslash \{\ell\}} g_\lambda$
            $v_i \leftarrow v_t$
        end for
    end for
    $G \leftarrow G \cup \{\mathbf{z}\}$
    $\overline{V} \leftarrow \overline{V} + \overline{V}_{\mathbf{z}}$
    $V \leftarrow V + z_m \overline{V}_{\mathbf{z}}$
end for

Figure 1.5: **Computing the hypervolume of a 3D frontier: first three iterations of the algorithm**. Consider a three-dimensional frontier Z. We sequentially add solutions to a 2D projection of the frontier, seen here (process moves from left to right). The solutions are added in order of decreasing value in their third component (height – not seen here). At each iteration, we compute the contribution in 2D as follows: Add the product of the solution's 2D components (the union of the yellow and gray areas). Then subtract all the previous existing frontier area (the union of the gray and white areas). Then add back the value of the sides (white areas). This yields the value of the yellow area. Multiply this value by the third component of the solution to obtain the solution's contribution to the hypervolume V.

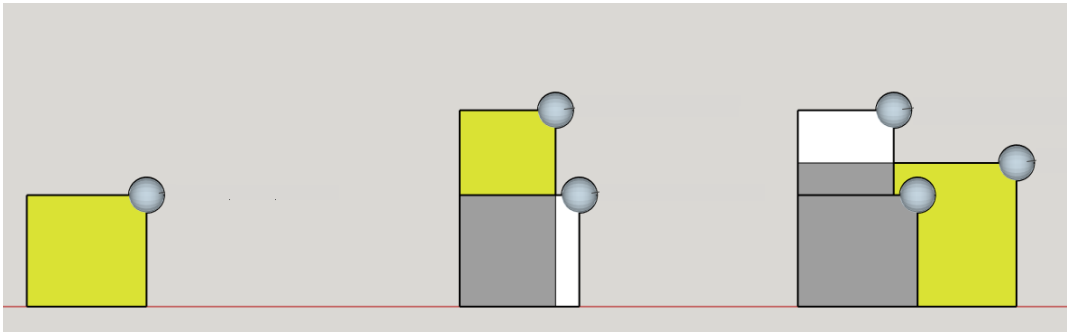

1.2.4 A new measure for pairwise objective conflict

When the hypervolume indicates that there is conflict in the system, how does the decision maker determine which objectives are responsible for the conflict? In the case of the hospital, is it cost and patient throughput that are most conflicting, or is it cost and required back-up? For the forest manager, are carbon sequestration and timber revenue the incompatible objectives responsible for the low hypervolume value, or is it wildlife habitat and timber revenue? If the forest manager oversees multiple independent forests, they may also ask whether the answers to these questions are the same in each. With the suite of measures currently available, the decision maker cannot adequately answer these questions. Here we propose a new measure of conflict to fill the void.

Consider the frontiers in Figure 1.6. The conflict between maximization objectives i and j is greatest in Frontier C and least in Frontier A.

Many authors have previously measured conflict between objectives [11][61][34], with

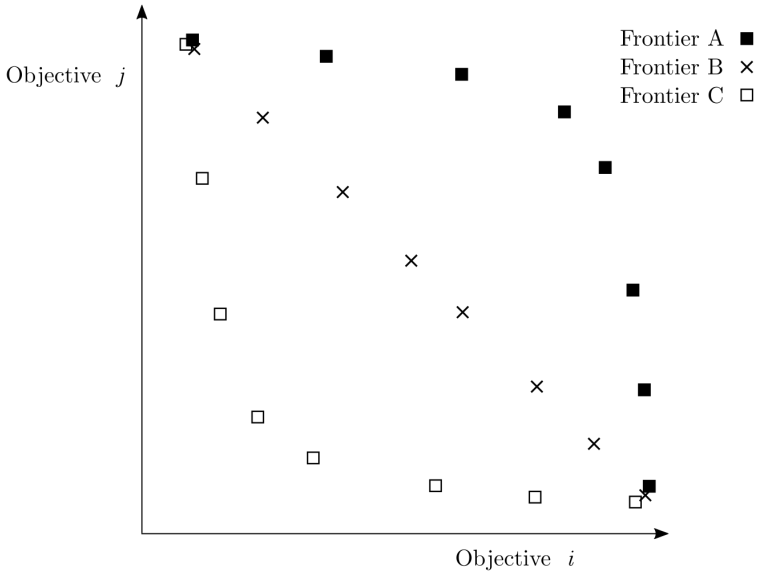

Figure 1.6: Varying conflict between objectives. The conflict between maximization objectives i and j increases from Frontier A to Frontier B to Frontier C.

most commonly used metrics deriving from measures of linear correlation (such as the Pearson correlation coefficient [23]) or rank correlation (such as Kendall's Tau [43] or Spearman's rho [45]). The motivation behind these metrics is often the removal of redundant objectives from a many-objective optimization problem. In such cases, measures of monotonicity or correlation alone suffice. However, the current metrics fall short of providing a quantification of conflict between pairs of objectives. Metrics for linear correlation are limited in their ability to capture the montonicity between objectives, which is the fundamental principle that determines if objectives conflict. Furthermore, both linear and rank correlation metrics fail to capture the objective achievement of the solutions. Thus, for a more nuanced understanding of the relationship between the objectives, a different metric is required.

Let $\mathbf{z}_{ij}$ be the sub-dimensional objective vector comprised of only the components corresponding to the ith and jth objectives $\mathbf{z}_{ij} = [z_i, z_j]$. We define the following measure of

conflict between objectives i and j:

$$C_{ij} = \frac{(1-\rho_{ij})\bar{d}_{ij}}{2d_{\max,ij}} \tag{1.17}$$

where $\bar{d}_{ij}$ is the average sub-dimensional distance from objective vectors to the ideal solution:

$$\bar{d}_{ij} = \frac{1}{|Z|}\sum_{\mathbf{z}\in Z} ||\mathbf{z}_{ij}^{\text{ideal}} - \mathbf{z}_{ij}|| \tag{1.18}$$

and

$$d_{\max,ij} = ||\mathbf{z}_{ij}^{\text{ideal}} - \mathbf{z}_{ij}^{\text{nadir}}|| \tag{1.19}$$

and ρ_{ij} is Spearman's rank-correlation coefficient for the solutions' achievements in objectives i and j. Note that $C_{ij} \in [0, 1)$, taking smaller values when there is less conflict between objectives i and j and larger values when there is more.

The conflict metric proposed here (equation (1.17)) addresses two major issues:

1. **Indifference to non-conflicting relationships**. Per equation (1.13), when an objective i increases monotonically with another objective j, the objectives do not conflict. Accordingly, C_{ij} should equal 0 in all such cases. This is true for the new metric, since for monotonically increasing objectives $\rho_{ij} = 1$, so $1 - \rho_{ij} = 0$.

2. **Consideration of objective achievement**. Recall Figure 1.6 and the intuitive notion that the conflict between objectives i and j is stronger in Frontier C than it is in Frontier B than it is in Frontier A. This notion is guided by the idea that the closer objective vectors are to the sub-dimensional ideal solution on average, the less the conflict between the objectives; that is, that greater simultaneous objective provision is indicative of less conflict. The proposed metric accounts for this, while correlation measures do not. In the extreme case of monotonically decreasing objectives, $\frac{(1-\rho_{ij})}{2} = 1$, so $C_{ij} = \frac{\bar{d}ij}{d_{\max,ij}}$. See Figure 1.7 for an example.

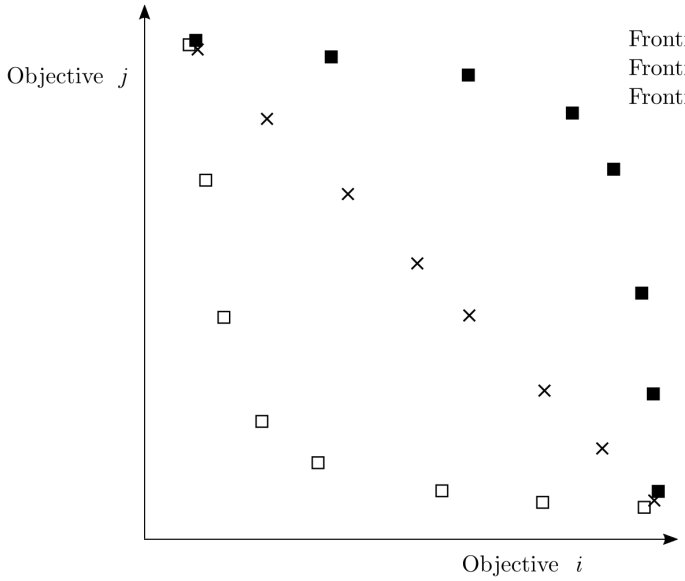

	Proposed C_{ij}	Pearson ρ_{ij}	Spearman $\rho_{s,ij}$
Frontier A	*0.4*	*-0.6*	*-1*
Frontier B	*0.6*	*-1*	*-1*
Frontier C	*0.8*	*-0.6*	*-1*

Figure 1.7: Comparing the proposed metric for conflict C_{ij} against the Pearson product-moment and the Spearman rank correlation coefficients (ρ_{ij} and $\rho_{s,ij}$, respectively). While the latter two are identical for frontiers A and C, the proposed metric is greater for frontier C than it is for A. This is because it accounts for the average relative distance to the sub-dimensional ideal objective vector.

To interpret differences in C_{ij} for different objective pairs, we decompose the metric into components: one for rank correlation

$$c_{ij,\rho} = \frac{1 - \rho_{ij}}{2}, \tag{1.20}$$

and one for objective achievement

$$c_{ij,d} = \frac{\bar{d}ij}{d_{\max,ij}}. \tag{1.21}$$

The components for different objective pairs (i, j) can be used to determine whether the

1.3 Case Study

To demonstrate the application of the hypervolume indicators and the proposed pairwise objective metric to the analysis of conflict in multi-objective systems, we perform a case

study on forest management in the Deschutes National Forest. We compare the conflict among ecosystem services in three multi-objective systems: one in which climate change is ignored, one in which climate change is predicted to be mild, and one in which it is predicted to be severe. For each climate change scenario, we solve a multi-objective mathematical program that optimizes ecosystem service achievement. The model aims to minimize fire hazard and sediment delivery while maximizing habitat for the northern spotted owl. In the coming sections we describe the study area and the importance of each of these ecosystem services. We then formally define the mathematical program solved for each climate change scenario and describe the climate scenarios considered.

1.3.1 Study area and selection of ecosystem services

To provide context for the selection of ecosystem services for the model, we first describe the area in which the case study was conducted. The area is known as the Drink Planning Area. It consists of 7056 ha of federally owned forest land on the east slopes of the Cascade Mountain Range located within the Deschutes National Forest. See Figure 1.8. Having never undergone logging or treatment, the Drink contains large areas of old growth forest. The large swaths of old growth forest in the Drink make it prime habitat for the northern spotted owl (NSO) (*Strix occidentalis caurina*, Figure 1.9), an iconic inhabitant of Pacific Northwest forests that is listed as a federally threatened species [14]. However, the same old growth conditions that render the area suitable habitat for the NSO also render it susceptible to high-severity wildfires. Such a wildfire would put at risk the NSO's habitat [16] as well as one of the Drink's other notable features - the municipal watershed for the cities of Bend, OR and Sisters, OR. Wildfires pose a threat to these cities' water supply, because they can cause soil water repellency, surface runoff, and debris torrents [41] which degrade watershed quality.

For these reasons, the managing entity, the United States Forest Service (USFS), would like to perform fuel removals in the Drink in order to reduce the area's fire hazard. However, performing these fuel removals has the potential to disrupt the habitat of the NSO [8] and to

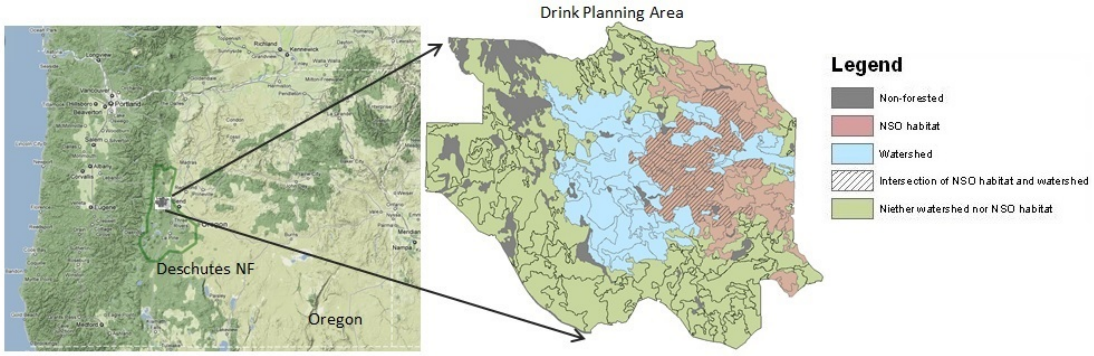

Figure 1.8: Overview of the study system, the Drink Planning Area, consisting of 7056 ha in the Deschutes National Forest. The Drink Area contains old growth forest that make it suitable habitat for the northern spotted owl. It also houses the municipal watershed for Bend, OR and Sisters, OR.

induce short-term increases in sediment delivery [57]. The latter is expected to be especially true in the Drink Area, where local USFS staff have noted that the watershed is unusually susceptible to spikes in sediment delivery as a result of foot traffic and other activities that occur within the watershed.

We developed a multi-objective mathematical program that optimizes the joint provision of these conflicting ecosystem services[1].

1.3.2 The multi-objective model

The multi-objective model is a zero-one mathematical program that assigns spatiotemporal prescriptions for fuel removals across the Drink Area to optimize the joint provision of ecosystem services. Spatially, the model assigns prescriptions across 303 forest stands into which the Drink has been divided (the interior polygons in Figure 1.8). Temporally, the

[1]These represent only a subset of the ecosystem services of concern to the USFS in the Drink Area. While the USFS manages for many services simultaneously, many of the services are stacked rather than bundled, meaning the ecosystem services are not in conflict. These services need not all be considered in the multi-objective model, because the selection and maximization of one ecosystem service entails the maximization of all in the stack. For this reason, we have disregarded non-conflicting ecosystem services and selected a minimal bundle on which to employ multi-objective optimization. Those that do not conflict can be stacked post-optimization.

Figure 1.9: The northern spotted owl is a threatened species whose habitat includes forests in the Pacific Northwest, including the Drink Area.

model operates over an 80-year planning horizon, from 2015 to 2095. The fuel removals are scheduled in two 20-year treatment periods: 2015-2035 and 2035-2055. For each stand, the model may prescribe fuel removals in the first period, the second period, neither, or both.

The model minimizes the fire hazard rating of the Drink Area at the end of the 80-year planning horizon, maximizes the area of NSO habitat at the end of each planning period, and minimizes the short-term spikes in sediment delivery resulting from the application of fuel removals. Fuel removals are assumed to be performed at the midpoint year in the treatment periods (years 2025 and 2045). Figure 1.10 contains a schematic of the planning horizon which shows the time of these events.

In the development of the model, we use the following notation.

Model parameters

- $i \in I$**:** the set of forest stands comprising the Drink Area ($|I| = 303$)

- a_i**:** the area of stand i

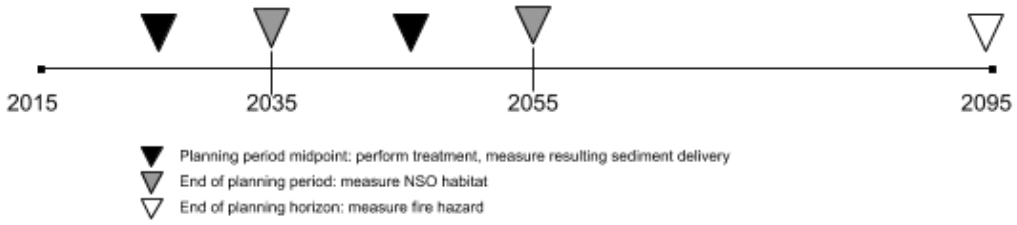

Figure 1.10: The planning horizon used in the case study spans the 80 year period from 2015 to 2095. Treatments may be performed in the first period, the second period, both, or neither. Treatments are assumed to be performed at the mid-point years of each period (black triangles). Sediment delivery is measured on treatment years. Stands' suitability for NSO habitat is measured at the end of the planning periods (gray triangles), and stands' fire hazard ratings are measured at the end of the planning horizon (white triangle).

- $r \in R$**:** the set of fuel removal prescriptions:

$$r = \begin{cases} 1 & \text{treatment applied in the first period (2015-2035)} \\ 2 & \text{treatment applied in the second period (2035-2055)} \\ 3 & \text{treatment applied in both periods} \\ 0 & \text{no treatment applied in either period} \end{cases}$$

- $F_{i,r}$**:** the area-weighted fire hazard rating of stand i at the end of the planning horizon if prescribed to fuel removal schedule r. The metric for fire hazard rating used in this analysis originated in the work by Schroder *et al.* [66]. This metric was developed for the Drink Area. It uses fire characteristics from the set of fuel models proposed by Anderson [4] in order to assign a fire hazard rating. I expanded the rating system to include fuel models not present in Schroder *et al.* See Table 1.1.

  The USFS's Climate-Forest Vegetation Simulator (Climate-FVS) was used to generate the fuels and vegetation characteristics of the stands in order to determine their fire hazard rating. Initial vegetation data for Climate-FVS came from the 2012 GNN structure map (`http://lemma.forestry.oregonstate.edu/data/structure-maps`) from Oregon State University's Landscape Ecology, Modeling, Mapping & Analysis

(LEMMA) group. Plots from the LEMMA database were mapped to the stands in the Drink area in order to produce tree and stand lists. These lists were used with Climate-FVS to simulate the stands' vegetation and fuels characteristics forward for the duration of the planning horizon under each climate scenario. Input climate data for Climate-FVS was obtained through the Climate-FVS climate data server [18].

Fuel Model	**Fire Hazard Rating**	Group	Flame length (m)	Rate of spread (m/hr)	Total fuel load (tons/ha)
4*	**5**	Shrub	5.79	1508.76	32.12
5	**4**	Shrub	1.22	362.10	8.65
8	**1**	Timber	0.30	32.19	12.36
9*	**2**	Timber	0.79	150.88	8.65
10	**2**	Timber	1.46	158.92	29.65
11*	**2**	Logging Slash	1.07	120.7	28.42
12	**4**	Logging Slash	2.44	261.52	85.50
13	**5**	Logging Slash	3.20	271.58	143.57

Table 1.1: Fire hazard rating system used here, originally employed by Schroder *et al.* [66]. Asterisks (*) denote fuel models not present in Schroder *et al.*
The fuel model column refers to the Anderson fuel model ratings [4].

- $I_{\omega,t}$**:** the set of stands that qualify as NSO habitat at the end of planning period t under at least one fuel removal schedule. The stands that qualify as NSO habitat at the end of a planning period t are those that meet the following three criteria, as specified by the USFS:

  1. elevation less than 1830 m
  2. the presence of trees with diameter at breast height (DBH) at least than 76 cm
  3. canopy closure of at least 60%

  The elevation requirement was checked using a digital elevation model from the US Department of Agriculture's GeoSpatial Data Gateway; canopy closure and large tree

criteria were determined using the simulated vegetation characteristics output from Climate-FVS.

To account for the large habitat requirements of the NSO, stands must also be members of a cluster exceeding 200 ha in size, the entirety of which meets the aforementioned NSO habitat criteria. Stands that meet the first three criteria but are not part of such a cluster are less valuable NSO habitat and therefore have their contributions to the total owl habitat discounted by a factor of e.

- e**:** the discount factor applied to NSO habitat when it is not part of a contiguous habitat cluster at least 200 ha in size. Following the convention used in Schroder *et al.* [66], we set $e = 0.5$.

- $j \in R_{i,t}$**:** the set of fuel removal schedules such that stand i qualifies as NSO habitat at the end of planning period t. For instance, consider stand $i = 15$ and planning period $t = 2$ (2035-2055). We seek to find the set of fuel removal prescriptions $r \in R$ such that stand 15 is suitable NSO habitat at the end of planning period 2 (in year 2055). We enumerate the vegetation characteristics of stand 15 for all possible fuel removal schedules and determine that if fuel removals are assigned in the second planning period, then stand 15 does not qualify as NSO habitat in year 2055. Thus, $R_{15,2} = \{0, 1\}$, since for $r = 0$ (no fuel removals performed) and $r = 1$ (fuel removals performed in first period only), stand 15 does qualify as NSO habitat in 2055.

- $s_{i,t}$**:** the amount of sediment (in tons) delivered to the watershed as a result of performing fuel removals on stand i in planning period t. The contributions of sediment delivery from treatment of stand i in period t were determined using the online GIS tool for the Watershed Erosion Prediction Project (WEPP) [32]. This tool takes soil textures, treatment types, duration of simulation, and custom climate data as inputs. Soil texture data for the Drink area was obtained from the USDA's Soil Survey Geographic (SSURGO) database, treatment types are those specified in §A, and the years

of simulation correspond to the treatment years in the planning horizon (2015-2095). The custom climate data are those described above for use with Climate-FVS, obtained through the Climate-FVS data server.

- $c \in C$**:** Recall that the quantification of NSO habitat depends on the availability of large contiguous habitat patches; areas of NSO habitat less than than 200 ha in size are discounted. In order to determine when habitat is provided in sufficiently large areas, we must enumerate the set of clusters of stands whose combined area exceeds 200 ha. This set of clusters is the set C.

- $i \in D_c$**:** Given a cluster $c \in C$, the set D_c is the set of stands that comprise cluster c.

- $c \in C_i$**:** Given a stand i, we define the set C_i as the set of clusters that contain stand i

- A**:** the maximum area in hectares that may be treated in either planning period. We constrain the allowable treatment area per period to account for the limited availability of work crews to perform the fuel removals. Following guidance from the USFS, we set $A = 2428$ ha (approximately 6000 ac).

- ℓ**,** u**:** the lower and upper bounds, respectively, on the relative fluctuation in the area treated in periods 1 and 2. These bounds are used to enforce regulation in the workflow for the USFS. Here we use values such that the area for which fuel removals are performed does not fluctuate more than 20% between treatment periods; that is, we set the lower bound $\ell = 0.8$ and the upper bound $u = 1.2$.

Decision Variables

$$x_{i,r} = \begin{cases} 1 & \text{if stand } i \text{ is prescribed to treatment schedule } r \\ 0 & \text{otherwise} \end{cases}$$

Indicator Variables

- $q_{c,t} = 1$ if all stands in cluster c qualify as NSO habitat at the end of planning period t; $q_{c,t} = 0$ otherwise

- $p_{i,t} = 1$ if in planning period t stand i is part of a cluster c such that $q_{c,t} = 1$; $p_{i,t} = 0$ otherwise

Accounting Variables

- S_t**:** the total sediment delivered to the watershed from performing fuel treatments in planning period t

- O_t**:** the amount of NSO habitat (in hectares) at the end of planning period t

- H_t**:** the total area (in hectares) treated in planning period t

1.3.3 Model formulation

The formulation of the multi-objective model is as follows:

$$Minimize$$

$$\sum_{i \in I} \sum_{r \in R} F_{i,r} x_{i,r} \tag{1.22}$$

$$\max\{S_1, S_2\} \tag{1.23}$$

$$Maximize$$

$$\min\{O_1, O_2\} \tag{1.24}$$

Subject to:

$$\sum_{i \in I_{\omega,t}} \left(a_i p_{i,t} + e a_i \left(\sum_{j \in R_{i,t}} x_{i,j} - p_{i,t} \right) \right) = O_t \qquad \forall t \in \{1,2\} \tag{1.25}$$

$$\sum_{i \in I} \sum_{r \in 1,3} s_{i,1} x_{i,r} = S_1 \tag{1.26}$$

$$\sum_{i \in I} \sum_{r \in 2,3} s_{i,2} x_{i,r} = S_2 \tag{1.27}$$

$$\sum_{i \in D_c} \sum_{j \in R_{i,t}} x_{i,j} - |c| q_{c,t} \geq 0 \qquad \forall t \in \{1,2\}, c \in C \tag{1.28}$$

$$\sum_{c \in C_i} q_{c,t} - p_{i,t} \geq 0 \qquad \forall t \in \{1,2\}, i \in I_{\omega,t} \tag{1.29}$$

$$\sum_{r \in R} x_{i,r} = 1 \qquad \forall i \in I \tag{1.30}$$

$$\sum_{i \in I} \sum_{r \in 1,3} a_i x_{i,r} = H_1 \tag{1.31}$$

$$\sum_{i \in I} \sum_{r \in 2,3} a_i x_{i,r} = H_2 \tag{1.32}$$

$$H_t \leq A \qquad \forall t \in \{1,2\} \tag{1.33}$$

$$\ell H_1 - H_2 \leq 0 \tag{1.34}$$

$$-u H_1 + H_2 \leq 0 \tag{1.35}$$

$$x_{i,r}, p_i, q_c \in \{0,1\} \quad \forall i \in I, r \in R, c \in C \tag{1.36}$$

Equations (1.22)-(1.24) are the objective functions: equation (1.22) minimizes the cumulative fire hazard rating of the Drink Area at the end of the 80-year planning horizon, equation (1.23) minimizes the maximum peak in sediment delivery for the two planning periods, and equation (1.24) maximizes the minimum NSO habitat available at the end of the planning periods. Equation set (1.25) defines the amount of NSO habitat available at the end of the planning horizons. Note that if stand i does not belong to a cluster of NSO habitat exceeding 200 hectares, then its area contribution to total NSO habitat is discounted by a factor of e. Equations (1.26) and (1.27) define the sediment delivered in planning periods

one and two, respectively.

Inequality set (1.28) controls the value of the cluster variables $q_{c,t}$ indicating clusters that meet the NSO habitat criteria in each of the planning periods. Inequality set (1.29) controls the value of the $p_{i,t}$ variables indicating whether stand i is included in a cluster of NSO habitat at time t.

The set of equalities (1.30) enforces the logical constraint that each stand must be prescribed to exactly one fuel removal schedule. Equations (1.31) and (1.32) are accounting constraints for the total area treated in each planning period, and inequalities (1.33) ensure that this area does not exceed the predefined maximum. Inequalities (1.34) and (1.35) bound the fluctuation in treated area between the planning periods. Finally, constraint (1.36) defines the decision and indicator variables as binary.

1.3.4 Solution method

We developed an implementation of Tóth's Alpha-Delta algorithm [73] to solve the model (1.22)-(1.36) utilizing the IBM ILOG CPLEX optimization engine. For a problem with M objectives, the Alpha-Delta algorithm finds the optimal set of solutions by iteratively slicing the M-dimensional objective space with a tilted $M-1$-dimensional hyperplane. The algorithm was implemented using an alpha parameter of $\alpha = .01$ and delta parameters of $\delta_{Hab} = 1$ ha and $\delta_{Sed} = 2$ tons for the NSO habitat and sediment delivery objectives, respectively.

1.3.5 Climate change scenarios

Like other ecosystems, forests will undergo changes as a result of the changing climate. For instance, researchers anticipate new spatial distributions of tree species [42], increased sediment delivery to streams [36], and increasing disturbance regimes such as wildfires, droughts, and insect infestations [79]. As these transformations occur, the ability of forests to provide ecosystem services will change.

The extent of change will likely depend on the severity of the realized climate change. Thus, to understand the potential impacts on ecosystem services, multiple climate change scenarios representing a range of severities should be considered. We use three in our case study: one scenario in which climate change is ignored, "None"; one in which climate change is predicted to be mild, "Ensemble RCP 4.5" (also "E45"); and one in which climate change is predicted to be severe, "Ensemble RCP 8.5" (also "E85"). These scenarios differ in their assumptions for the additional energy per unit area that will be absorbed by the atmosphere, a value known as radiative forcing (RF). E45 assumes 4.5 W/m^2 and E85 assumes 8.5 W/m^2. In general, larger values of RF correspond to more severe climate change.

A given value for radiative forcing does not map to a single prediction of climate change, because researchers may disagree in how the climate will respond to a given amount of RF. This is why for a given RF numerous climate models exist. A common approach to handling the disagreement among the climate models is to use an ensemble of climate models that all assume the same RF. We adopt this approach here for our E85 and E45 scenarios.

Each of these scenarios corresponds to an ensemble of 17 climate models. These climate models originate from the Fifth Assessment (AR5) on climate performed by the Intergovernmental Panel on Climate Change (IPCC). The selection and assembly of the 17 climate models used in these ensembles was conducted by Cookston (2016) and the Climate-FVS team [17].

The other scenario, None, ignores any effects of climate change. While the number of studies incorporating climate change is increasing, this is still a common assumption in modern studies such as Schroder *et al.* (2013) [66]. Because it has served as the basis for many past studies of ecosystem services, the None climate scenario serves as a control against which we will compare the other two.

Each climate scenario corresponds to a different parameterization of the model, since the vegetation, fuels, and sediment delivery data depend on climate. Thus, changing the climate scenario has the potential to affect the amount and location of NSO habitat, the effects of fuel removals on NSO habitat, the fire hazard of the Drink Area, the efficacy of the fuel

Table 1.2: Summary of the performance of the efficient frontiers for each climate change scenario.

		None	**E45**	**E85**
Fire hazard	min	21321.21	23219.82	23268.02
	max	21933.29	23973.79	23724.98
	avg	21406.26	23324.41	23369.57
NSO habitat	min	2532.33	2412.18	2171.10
	max	2540.05	2477.18	2481.01
	avg	2536.31	2447.92	2421.99
Sediment delivery	min	0	0	0
	max	24.57	63.43	69.68
	avg	10.25	27.98	31.19

removals in reducing fire hazard, and the sediment delivered as a result of fuel removals. This drives changes to the relationships among the ecosystem services as well.

1.3.6 Results

We parameterized and solved the multi-objective model ((1.22)-(1.36)) for each of the climate scenarios, generating three efficient frontiers: Z_{None}, Z_{E45}, and Z_{E85} for the None, Ensemble RCP 4.5, and Ensemble RCP 8.5 scenarios, respectively. Figure 1.11 shows the frontiers in their 3-dimensional objective spaces while Figure 1.12 provides a parallel coordinates view of the frontiers; their summary details are listed in Table 1.2.

We begin our analysis by investigating the impacts of climate change on the provision of individual ecosystem services. We then consider how climate change impacts the joint provision of ecosystem services and the conflict among them.

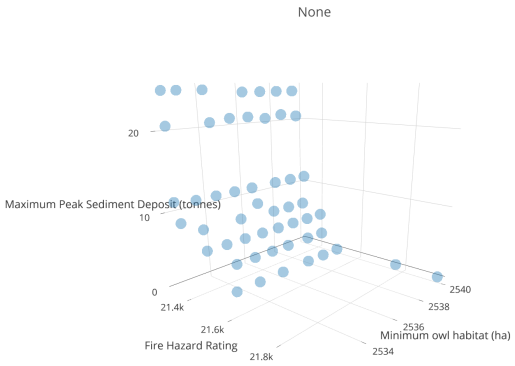

(a) None

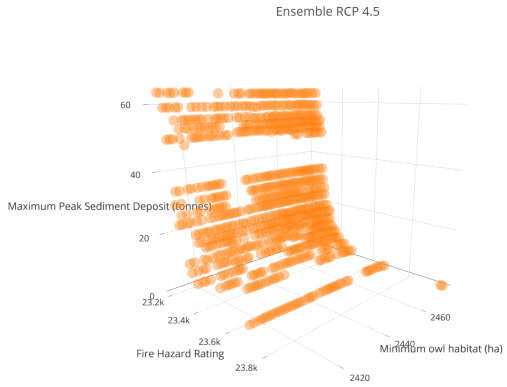

(b) Ensemble RCP 4.5

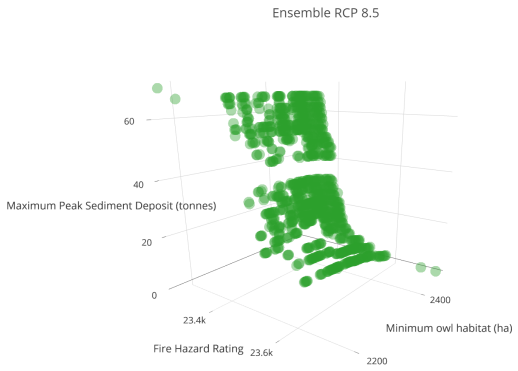

(c) Ensemble RCP 8.5

Figure 1.11: Efficient frontiers for each climate change scenario.

Provision of individual ecosystem services

The average achievement of all ecosystem services decreases with increasing severity of climate change (see Table 1.2, "avg" rows). We find that the difference in ecosystem service provision is greater between the assumption of no climate change and mild climate change (None to E45) than it is between mild climate change and severe climate change (E45 to E85). This suggests that, for the ecosystem services in this study, the realization of climate change is more significant than the severity of that change. The model data provide evidence

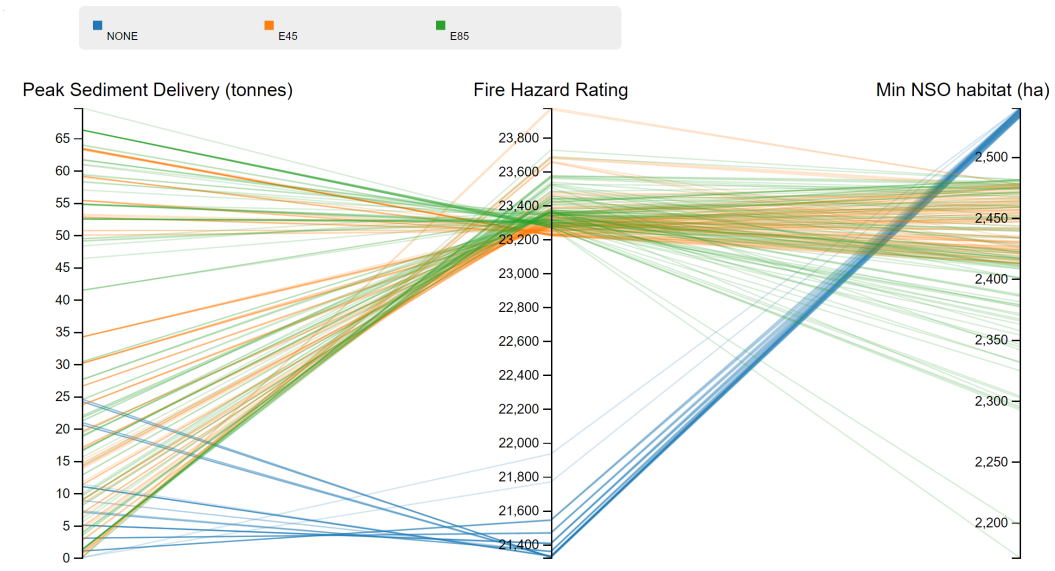

Figure 1.12: Parallel coordinates view of the frontiers. Each axis represents an ecosystem service optimized by the model and each line a solution. In all objectives, we notice that None appears to outperform both the E45 and E85 scenarios, which show similar average objective achievements. To increase visual clarity, only a subset of solutions for E45 and E85 are shown because of the number of solutions in these frontiers.

of why this is the case.

Sediment delivery Compared to the None scenario, the average amount of sediment delivered is 172% higher in E45 and 204% higher in E85. To understand why this may be, consider Figure 1.13. The figure shows the average tonnes of sediment delivered as a result of performing fuel removals for each climate change scenario. The sediment delivery per fuel removal under E45 is nearly twice the sediment delivery under the None scenario (81% higher), whereas the E85 scenario is only 0.4% higher than the E45 scenario.

This is a result of the response in sediment delivery to prescribed burns and the frequency with which they are assigned[2]. Our simulations show that increasing the severity of climate change causes pronounced increases in sediment delivery as a result of prescribed burns. We

[2]For additional information on how stands are assigned a specific fuel removal technique such as thinning or prescribed burn, see the appendix, §A.

also find that relative to the None scenario, prescribed burns are assigned more frequently in the climate change scenarios: 8 times more frequently in E45 and 10.1 times more frequently in E85. See Table 1.3. These effects combine to produce the result seen in Figure 1.13 of increasing sediment levels with climate change severity.

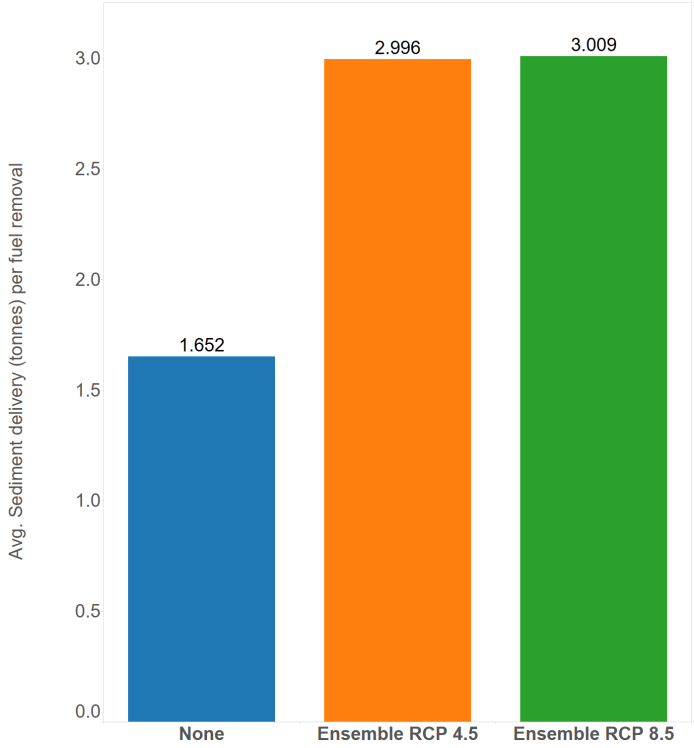

Figure 1.13: Average spike in sediment delivery as a result of performing fuel removals for each of the climate change scenarios.

Fire hazard Similarly, we find that the average fire hazard of the Drink Area increases with climate change severity, with E45 and E85 both performing approximately 9% worse than None. First, we note that this is not due to the model simply selecting less area for treatment under the climate change scenarios, as this value is essentially constant across both treatment periods and all climate scenarios (see Table 1.4). Instead, we find that the increase in fire hazard is due to the impact of climate change on the fuel model classification

Table 1.3: Frequency and impact of prescribed burn for each climate scenario. The combination of more frequent prescribed burns and increased sediment delivery per prescribed burn results in the higher values of sediment delivery in E45 and E85 observed in Figure 1.13.

	None	**E45**	**E85**
Average sediment delivery (tonnes) from prescribed burn	31.23	48.56	48.97
Number of prescribed burns assigned	34	272	344

Table 1.4: Areas treated per period across climate scenarios. The values are nearly the same for both periods and for each climate scenario.

	None	**E45**	**E85**
Area treated (ha) in period 1	2427.31	2426.90	2414.58
Area treated (ha) in period 2	2427.56	2427.71	2427.63

of the stands in the Drink Area. In E45 and E85, more stands are assigned a fuel model classification that is associated with higher fire hazard (refer to table 1.1 for the mapping from fuel model to fire hazard). This is shown in Figure 1.14, where we observe a larger percentage of stands having a fire hazard rating of either 4 or 5 under the E45 and E85 scenarios than in None.

NSO habitat Finally, we also observe a decrease in the average provision of NSO habitat under the consideration of climate change. The average provision in the E45 scenario is 88.4 ha less than in None, and E85 is 114.3 ha less. The result is largely due to the effects of climate change on the vegetation characteristics that define whether a stand qualifies as NSO habitat. Of the criteria used, two of them are determined by vegetation characteristics: the presence of at least one tree with DBH > 76 cm and canopy closure of at least 60%. While climate change has minimal impact on the former, the average canopy closure for stands in

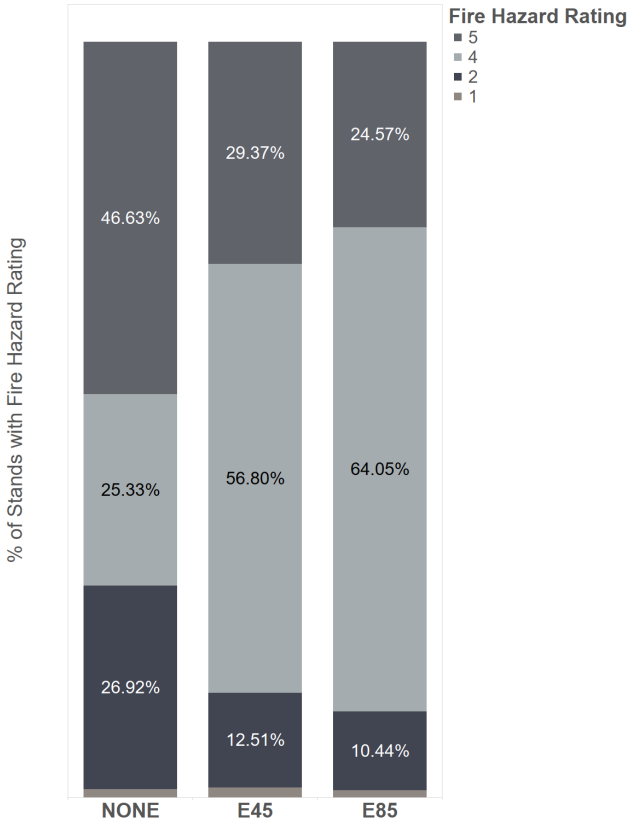

Figure 1.14: Distributions of fire hazard ratings across the Drink Area under each climate change scenario. Moving from left to right (in increasing climate change severity), we observe an increase in the number of stands classified with more extreme fire hazards (ratings of 4 and 5).

the Drink Area decreases with increasing severity of climate change. See Figure 1.15.

We also find that the range of achievable values of NSO habitat increases with climate change severity. There are two primary drivers for this increase. The first is in the impact of fuel removals on the amount of NSO habitat available. We see in Table 1.5 the number of instances in which performing a fuel removal disqualifies a stand from being NSO habitat under each climate change scenario. This happens more than twice as frequently in E45 and E85 than in None. Second, we find that the reduction in fire hazard that results from performing a fuel removal which leads to the disqualification of NSO habitat increases with

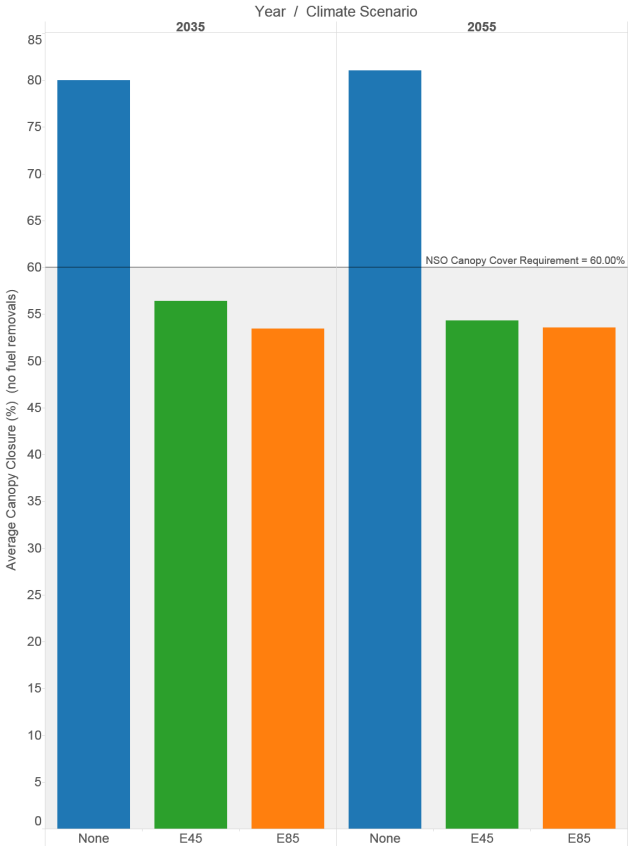

Figure 1.15: Average canopy closure for stands in the Drink Area for each climate scenario. Shown are canopy closure values during years 2035 and 2055 (the years in which NSO habitat is measured) when no fuel removals are performed. We see that with increasing climate change severity, canopy closure decreases.

climate severity. That is, the model is more incentivized to sacrifice NSO habitat in favor of fire hazard reduction. This in turn leads to a reduction in clustering of NSO habitat, further reducing the objective function value (equation (**??**)). This data is shown in Figure 1.16, in which we see the reduction in fire hazard as a result of fuel removals that disqualify a stand as NSO habitat. These values increase with climate change severity.

We next consider how climate change impacts the joint provision of ecosystem services and the conflict among them.

Table 1.5: Shown here are the number of times for each climate scenario that a fuel removal triggers the disqualification of a stand from being NSO habitat.

Climate change scenario	**Disqualifications of NSO habitat as a result of fuel removals**
None	24
Ensemble RCP 4.5	63
Ensemble RCP 8.5	67

Table 1.6: Hypervolume for each climate change scenario. Hypervolume values increase with increasing severity of climate change.

	None	**E45**	**E85**
Hypervolume	0.876977	0.866857	0.829541

Joint provision of ecosystem services

As we saw for provision of individual ecosystem services, our results show that climate change will have an impact on the joint provision of ecosystem services as well. We observe a decreasing hypervolume with increasing severity of climate change - see Table 1.6. A decreasing hypervolume is indicative of more conflict in the system, meaning that climate change is associated with more conflict among the ecosystem services.

The difference in hypervolume between None and E45 is approximately 0.01. Recall that a difference of h in hypervolumes equates to a difference of $h^{1/M}$ in each objective. Thus, despite the small size of the difference between $I_{H1}(Z_{\text{None}})$ and $I_{H1}(Z_{\text{E45}})$, it signifies an additional achievement in each objective of approximately 21.6%. The difference is greater between None and E85, approximately 0.05, which represents an additional achievement in each objective of 36.2%.

From the hypervolumes alone, it is uncertain whether None represents a strictly better frontier than either E45 or E85 or if, despite their smaller hypervolume values, E45 and E85

Table 1.7: Binary hypervolumes for each pair of climate scenarios. No values are negative, indicating that no frontiers are dominated by another and that all frontiers uniquely enclose some volume of the objective space.

Z_1	Z_2	$I_{H2}(Z_1, Z_2)$
None	**E45**	0.026154
None	**E85**	0.058001
E45	**None**	0.016034
E45	**E85**	0.045156
E85	**None**	0.010565
E85	**E45**	0.007841

enclose some region of the objective space that is not enclosed by None. Any such region would extend further into the objective space, representing the presence of solutions for whom greater joint provision of ecosystem services is possible. We use the binary hypervolume indicator I_{H2} to detect the presence and size of these regions. The binary hypervolume values for each pair of frontiers are shown in Table 1.7.

The binary hypervolume values tend to align with the hypervolume values, with larger values of $I_{H2}(Z_1, Z_2)$ when $I_{H1}(Z_1) > I_{H1}(Z_2)$ and smaller values when $I_{H1}(Z_2) > I_{H1}(Z_1)$. Interestingly, all binary hypervolume values are positive, indicating that no frontier is dominated by any other. This region of the objective space bound only by a frontier Z_i indicates the presence solutions in climate scenario i that achieve greater joint provision of ecosystem services.

To determine the location of these regions and better understand the basis of the change in conflict between climate scenarios, we examine pairwise objective relationships.

Sediment delivery-NSO Habitat We observe no clear relationship between climate change severity and the conflict between sediment delivery and NSO habitat; see Figure 1.17. The figure shows the efficient frontier plotted in the sediment delivery-NSO habitat

Table 1.8: Conflict between sediment delivery and NSO habitat across climate scenarios.

	C_{ij}	$c_{ij,\rho}$	$c_{ij,d}$
None	0.19639	0.3974	0.4942
E45	0.25667	0.5194	0.4941
E85	0.19284	0.5160	0.3737

plane, where each objective has been normalized such that better values are higher and worse values are lower. For instance, in this graph, the point $(1, 1)$ represents 0 sediment delivery and maximum NSO habitat. We see similar uniform spreads of solutions for each climate scenario.

The values for pairwise conflict also indicate a lack of conflict, as seen in Table 1.8. Values for C_{ij} are all less than 0.25, with the highest value for the E45 scenario and lower values for E85 and None.

To determine the reason for the variation in C_{ij} by climate scenario, we disassemble the conflict metric into components. A value of $c_{ij,\rho} = 0.5$ indicates the absence of rank correlation, and we find no climate scenario that differs significantly from this value. Lower values of $c_{ij,\rho}$ indicate positive rank correlation, such as in None ($c_{ij,\rho} = 0$ for non-conflicting objectives); higher values for $c_{ij,\rho}$ indicate more conflict. $c_{ij,d} \in [0, 1]$ represents the average distance of solutions from the sub-dimensional ideal solution. The solutions in the E45 and None scenarios are further away from the sub-dimensional ideal solution than those in E85 leading to larger values of $c_{ij,d}$, but all climate scenarios have on average solutions that are near the mid-point mark of $c_{ij,d} = 0.5$.

NSO habitat-fire hazard According to the conflict metric proposed here, the conflict between NSO habitat and fire hazard is small for all climate scenarios but appears to decrease with increasing severity of climate change. We find this is due primarily to the increasing density of solutions nearer the sub-dimensional ideal solution in the E45 and E85 scenarios

compared to None. See Figure ADDIN2DSLICEFIGURE. Breaking the conflict metric again into components (see Table MAKETHECOMPONENTRYTABLE), we see that the average distance to the ideal decreases with increasing severity of climate change, while the rank correlation again does not differ significantly from 0.5.

Fire hazard-sediment delivery In all climate scenarios, the strongest pairwise conflict is between fire hazard and sediment delivery. This is apparent from both Figure MAKE2DSLICEFIGURE and the conflict metric MAKECOMPONENTTABLE. All rank correlation conflict values $c_{ij,\rho} > 0.95$, indicating strong negative rank correlation. In Figure MAKE2DSlICEFIG we observe a clear void of solutions in all climate change scenarios near the sub-dimensional ideal solution at $(1, 1)$, unlike in Figures 1.17 and NSO-FIREFIGURE. We also notice that the None and E45 solutions generally extend beyond the E85 solutions in this plane.

All fuel removals on watershed stands induce sediment delivery - refer again to Figure (the figure which shows sed deliv per fuel removal) for the average sediment deposit per fuel removal. We can also consider the relative gain from performing these fuel removals. That is, what is the average reduction in fire hazard per tonne of sediment delivered? This is shown in Figure MAKEFIGFhREDUCPERTONNESED. Both of these figures show that increasing climate change severity should increase the conflict between fire hazard and sediment delivery as a result of the increased tradeoff in fire hazard per tonne of sediment delivered. We observe this, however, the conflict metric is not as different between the climate scenarios as we might expect given the results in these figures. This is due to the availability of watershed stands in the E45 and E85 scenarios for whom the sediment contribution is small relative to the total sediment delivered. Examples of solutions taking advantage of these stands are those in Figure 2DFIRESEDSLICE with sediment delivery > 0.9 and fire hazard < 0.7. However, the number of such stands is limited, and to continue to improve fire hazard, stands with larger resulting sediment deposits must be treated. Since the average sediment deposit is higher for the E45 and E85 scenarios, we see the steep drop beyond about 0.8 FH for E85

and 0.9 for E45. Notice, meanwhile, that None is a more gradual descent given the smaller variation in sediment delivery for fuel removals.

1.3.7 Discussion

MOVE A BUNCH OF STUFF FROM ABOVE DOWN HERE

1.4 Discussion & Conclusion

1.4.1 New conflict metric

- should this still stay here? probably. Try to keep wording non-specific to the case study, since some readers will have skipped it. Go with something like "We saw in the case study that the conflict metric was able to sniff out nuanced differences between objectives across multi-obj systems..." or soemthing else awesome like that.

Pros We saw that fire-sed relationship is very similar across climate scenarios, and the metric captures this. However, it even succeeds in capturing the nuanced "gets worse with climate change" even though its slight. Man o man. Also, it gives a higher conflict value for fire-sed than it does to either of the other obj pairs, which is good, bc there's more conflict there. The others are more scattered, and it gives low values for these. However, it might be that it isn't as good as sniffing out conflict among minimally conflicting objective pairs. It tends to vary a lot for the scattered ones, although that can be justified too, since the sols in that one plot show that E85 spends less time near the bad values, so really, I mean, it's OK.

Cons When looking at all pairwise conflict metrics for a frontier, their combination does not let you make deductions of the whole system level conflict. Weights average objective achievement perhaps too much. Frontiers with a bunch of solutions nearer the ideal are given less conflict. perhaps that's OK though.

TO TALK ABOUT SOMEWHERE: Why the disparity in number of solutions? Why E85 achieve relatively more NSO habitat and relatively less FH on average than the others (fig 1.17 and sim for NSO-FH)? The increased range in achievable values for the objs in the case of climate change leads to results that show tighter clustering closer to ideal, which weights the conflict towards "less". Basically, more extreme extremes make most other values seem more normal(?).

INVESTIGATE MORE: What's the difference in actual acreage of NSO hab vs diffs due to clustering discounts? Made that map, but don't want to talk about unless I'm encouraged (Sandor...) to talk about it. Make sure this sentence doesn't make it into my next draft. NUM SOLUTIONS = bc of the DQing of NSO hab as a result of actions, there are more combos of ways to do that and pvar values as a result. And so the model has to make more decisions about whether to make something owl habitat or instead do a treatment. And this leads to many more results that we didn't have before. And lots of constraints involve the pvars and qvars, and so this would mean harder to solve (which we saw but didn't talk about here). Also the

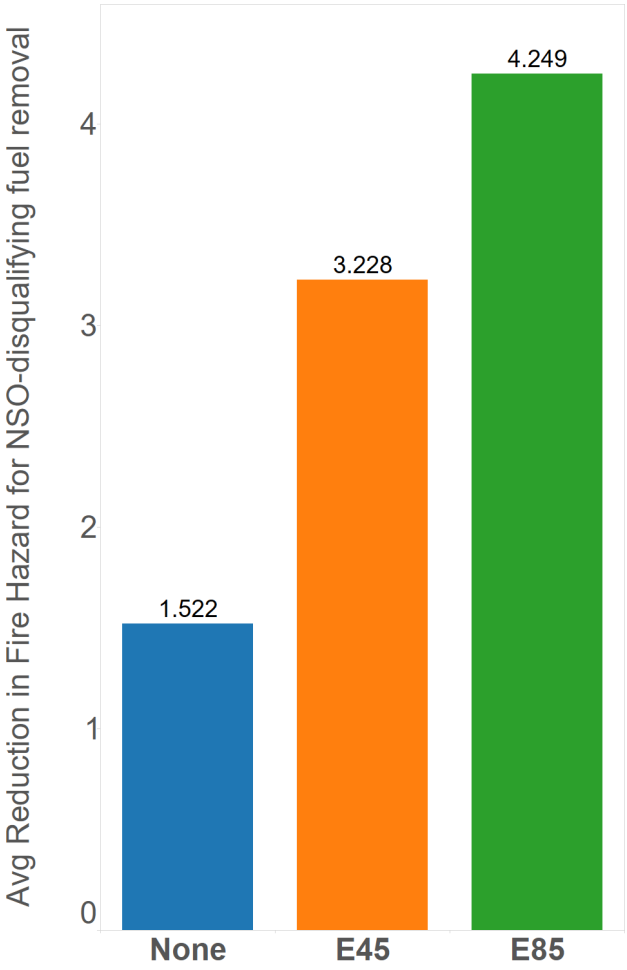

Figure 1.16: Some stands may always be NSO habitat and others may never be NSO habitat, regardless of model decisions. For those stands which vary based on model decisions, we see here the average efficacy of fuel removals which disqualify their being NSO habitat. This value increases with increasing climate change, indicating greater incentive for the model to forgo NSO habitat in favor of fire hazard reduction.

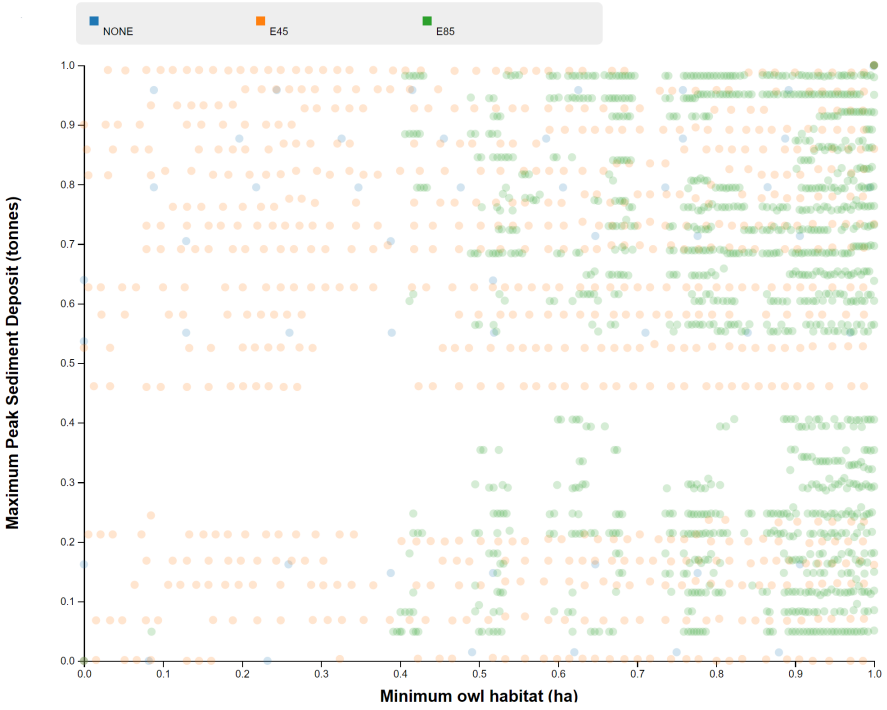

Figure 1.17: NSO habitat versus sediment delivery for all climate scenarios. No obvious conflict pattern exists between the objectives in any climate scenario.

BIBLIOGRAPHY

[1] 36 CFR 219.1. National forest system land management planning, 2012.

[2] Fouad Ben Abdelaziz. Solution approaches for the multiobjective stochastic programming. *European Journal of Operational Research*, 216(1):1–16, 2012.

[3] Frank A Albini. Estimating wildfire behavior and effects. 1976.

[4] Hal E Anderson. Aids to determining fuel models for estimating fire behavior. *The Bark Beetles, Fuels, and Fire Bibliography*, page 143, 1982.

[5] Millennium Ecosystem Assessment et al. *Ecosystems and human well-being*, volume 5. Island press Washington, DC:, 2005.

[6] Brad Bass, Guohe Huang, and Joe Russo. Incorporating climate change into risk assessment using grey mathematical programming. *Journal of Environmental Management*, 49(1):107 – 123, 1997.

[7] Gordon B Bonan. Forests and climate change: forcings, feedbacks, and the climate benefits of forests. *Science*, 320(5882):1444–1449, 2008.

[8] Monica L Bond, RJ Gutiérrez, Alan B Franklin, William S LaHaye, Christopher A May, and Mark E Seamans. Short-term effects of wildfires on spotted owl survival, site fidelity, mate fidelity, and reproductive success. *Wildlife Society Bulletin*, pages 1022–1028, 2002.

[9] Jose G Borges, Jordi Garcia-Gonzalo, Vladimir Bushenkov, Marc E McDill, Susete Marques, and Manuela M Oliveira. Addressing multicriteria forest management with pareto frontier methods: An application in portugal. *Forest Science*, 60(1):63–72, 2014.

[10] Dimo Brockhoff and Eckart Zitzler. Are all objectives necessary? on dimensionality reduction in evolutionary multiobjective optimization. In *Parallel Problem Solving from Nature-PPSN IX*, pages 533–542. Springer, 2006.

[11] Dimo Brockhoff and Eckart Zitzler. Objective reduction in evolutionary multiobjective optimization: Theory and applications. *Evolutionary Computation*, 17(2):135–166, 2009.

[12] Brett A. Bryan and Neville D. Crossman. Systematic regional planning for multiple objective natural resource management. *Journal of Environmental Management*, 88(4):1175 – 1189, 2008.

[13] Kai MA Chan, M Rebecca Shaw, David R Cameron, Emma C Underwood, and Gretchen C Daily. Conservation planning for ecosystem services. *PLoS biology*, 4(11):e379, 2006.

[14] US Congress. Endangered species act. *Washington DC*, 1973.

[15] Ira R. Cooke, Simon A. Queenborough, Elizabeth H. A. Mattison, Alison P. Bailey, Daniel L. Sandars, A. R. Graves, J. Morris, Philip W. Atkinson, Paul Trawick, Robert P. Freckleton, Andrew R. Watkinson, and William J. Sutherland. Integrating socio-economics and ecology: a taxonomy of quantitative methods and a review of their use in agro-ecology. *Journal of Applied Ecology*, 46(2):269–277, 2009.

[16] Steven P Courtney and Andrew B Carey. *Scientific evaluation of the status of the Northern Spotted Owl*. Sustainable Ecosystems Institute Portland, OR, 2004.

[17] Nicholas Crookston. Details of data and methods used for calculating future climate estimates, 2016.

[18] Nicholas Crookston. Get climate-fvs ready data, 2016.

[19] Nicholas L Crookston. Climate-fvs version 2: Content, users guide, applications, and behavior. 2014.

[20] Piotr Czyżżak and Adrezej Jaszkiewicz. Pareto simulated annealingâĂŤa metaheuristic technique for multiple-objective combinatorial optimization. *Journal of Multi-Criteria Decision Analysis*, 7(1):34–47, 1998.

[21] Gretchen C Daily, Susan Alexander, Paul R Ehrlich, Larry Goulder, Jane Lubchenco, Pamela A Matson, Harold A Mooney, Sandra Postel, Stephen H Schneider, David Tilman, et al. *Ecosystem services: benefits supplied to human societies by natural ecosystems*, volume 2. Ecological Society of America Washington (DC), 1997.

[22] Kalyanmoy Deb. *Multi-objective optimization using evolutionary algorithms*, volume 16. John Wiley & Sons, 2001.

[23] Kalyanmoy Deb and D Saxena. Searching for pareto-optimal solutions through dimensionality reduction for certain large-dimensional multi-objective optimization problems. In *Proceedings of the World Congress on Computational Intelligence (WCCI-2006)*, pages 3352–3360, 2006.

[24] Kalyanmoy Deb and Dhish Kumar Saxena. On finding pareto-optimal solutions through dimensionality reduction for certain large-dimensional multi-objective optimization problems. *Kangal report*, 2005011, 2005.

[25] Luis Diaz-Balteiro and Carlos Romero. Making forestry decisions with multiple criteria: a review and an assessment. *Forest Ecology and Management*, 255(8):3222–3241, 2008.

[26] Gary E Dixon et al. Essential fvs: A userâĂŹs guide to the forest vegetation simulator. *Fort Collins, CO: USDA-Forest Service, Forest Management Service Center*, 2002.

[27] German Climate Computing Centre (DKRZ). IPCC working group i AR5 snapshot.

[28] Oregon Fish and Wildlife Office. Species fact sheet: Northern spotted owl. `http://www.fws.gov/oregonfwo/Species/Data/NorthernSpottedOwl/default.asp`. Accessed: 2015-02-06.

[29] US Fish, Wildlife Service, et al. Revised recovery plan for the northern spotted owl (strix occidentalis caurina). *USDI Fish and Wildlife Service, Portland, OR USA*, 2011.

[30] Forestières Internationaler Verband Forstlicher Forschungsanstalten. Adaptation of forests and people to climate change. 2009.

[31] Eclipse Foundation. Eclipse, 2014.

[32] James R Frankenberger, Shuhui Dun, Dennis C Flanagan, Joan Q Wu, and William J Elliot. Development of a gis interface for WEPP model application to great lakes forested watersheds. In *International Symposium on Erosion and Landscape Evolution (ISELE), 18-21 September 2011, Anchorage, Alaska*, page 139. American Society of Agricultural and Biological Engineers, 2011.

[33] William L Gaines, Richy J Harrod, James Dickinson, Andrea L Lyons, and Karl Halupka. Integration of northern spotted owl habitat and fuels treatments in the eastern cascades, washington, usa. *Forest Ecology and Management*, 260(11):2045–2052, 2010.

[34] Tomas Gal and Heiner Leberling. Redundant objective functions in linear vector maximum problems and their determination. *European Journal of Operational Research*, 1(3):176–184, 1977.

[35] J Garcia-Gonzalo, JG Borges, JHN Palma, and A Zubizarreta-Gerendiain. A decision support system for management planning of eucalyptus plantations facing climate change. *Annals of Forest Science*, 71(2):187–199, 2014.

[36] Jaime R. Goode, Charles H. Luce, and John M. Buffington. Enhanced sediment delivery in a changing climate in semi-arid mountain basins: Implications for water resource management and aquatic habitat in the northern rocky mountains. *Geomorphology*, 139âĂŞ140(0):1 – 15, 2012.

[37] Lee E Harding and Emily McCullum. Ecosystem response to climate change in british columbia and yukon: threats and opportunities for biodiversity. *Responding to global climate change in British Columbia and Yukon*, 1:9–1, 1997.

[38] Grant Hauer, Steve Cumming, Fiona Schmiegelow, Wiktor Adamowicz, Marian Weber, and Robert Jagodzinski. Tradeoffs between forestry resource and conservation values under alternate policy regimes: A spatial analysis of the western canadian boreal plains. *Ecological Modelling*, 221(21):2590 – 2603, 2010.

[39] Anke K Hutzschenreuter, Peter AN Bosman, and Han La PoutrÚ. Evolutionary multiobjective optimization for dynamic hospital resource management. In *International Conference on Evolutionary Multi-Criterion Optimization*, pages 320–334. Springer, 2009.

[40] IPCC Working Group I. *Climate Change 2013-The Physical Science Basis: Summary for Policymakers*. Intergovernmental Panel on Climate Change, 2013.

[41] George G Ice, Daniel G Neary, and Paul W Adams. Effects of wildfire on soils and watershed processes. *Journal of Forestry*, 102(6):16–20, 2004.

[42] Louis R Iverson and Anantha M Prasad. Predicting abundance of 80 tree species following climate change in the eastern united states. *Ecological Monographs*, 68(4):465–485, 1998.

[43] Evangelos Kanoulas and Javed A Aslam. Empirical justification of the gain and discount function for ndcg. In *Proceedings of the 18th ACM conference on Information and knowledge management*, pages 611–620. ACM, 2009.

[44] Amit Kanudia and Richard Loulou. Robust responses to climate change via stochastic markal: The case of quÃľbec. *European Journal of Operational Research*, 106(1):15 – 30, 1998.

[45] Prasad Karande and Shankar Chakraborty. Application of multi-objective optimization on the basis of ratio analysis (moora) method for materials selection. *Materials & Design*, 37:317–324, 2012.

[46] Vineet Khare, Xin Yao, and Kalyanmoy Deb. Performance scaling of multi-objective evolutionary algorithms. In *Evolutionary Multi-Criterion Optimization*, pages 376–390. Springer, 2003.

[47] Joshua Knowles and David Corne. On metrics for comparing nondominated sets. In *Evolutionary Computation, 2002. CEC'02. Proceedings of the 2002 Congress on*, volume 1, pages 711–716. IEEE, 2002.

[48] Danny C Lee and Larry L Irwin. Assessing risks to spotted owls from forest thinning in fire-adapted forests of the western united states. *Forest Ecology and Management*, 211(1):191–209, 2005.

[49] Marcus Linder. Developing adaptive forest management strategies to cope with climate change. *Tree Physiology*, 20(5-6):299–307, 2000.

[50] Alexander V Lotov, Vladimir A Bushenkov, and Georgy K Kamenev. *Interactive decision maps: Approximation and visualization of Pareto frontier*, volume 89. Springer, 2004.

[51] Alexander V Lotov and Kaisa Miettinen. Visualizing the pareto frontier. In *Multiobjective optimization*, pages 213–243. Springer, 2008.

[52] B Luo, I Maqsood, YY Yin, GH Huang, and SJ Cohen. Adaption to climate change through water trading under uncertainty- an inexact two-stage nonlinear programming approach. *Journal of Environmental Informatics*, 2(2):58–68, 2003.

[53] Shunsuke Managi. Evaluation and policy analysis of japanese forestry. In *2005 Annual meeting, July 24-27, Providence, RI*, number 19358. American Agricultural Economics Association (New Name 2008: Agricultural and Applied Economics Association), 2005.

[54] Donald McKenzie, Ze'ev Gedalof, David L Peterson, and Philip Mote. Climatic change, wildfire, and conservation. *Conservation Biology*, 18(4):890–902, 2004.

[55] Robin Naidoo, Andrew Balmford, Robert Costanza, Brendan Fisher, Rhys E Green, B Lehner, TR Malcolm, and Taylor H Ricketts. Global mapping of ecosystem services and conservation priorities. *Proceedings of the National Academy of Sciences*, 105(28):9495–9500, 2008.

[56] Craig R. Nitschke and John L. Innes. Integrating climate change into forest management in south-central british columbia: An assessment of landscape vulnerability and development of a climate-smart framework. 2008.

[57] Jay OâĂŹLaughlin. Conceptual model for comparative ecological risk assessment of wildfire effects on fish, with and without hazardous fuel treatment. *Forest Ecology and Management*, 211(1):59–72, 2005.

[58] Intergovernmental Panel on Climate Change. Definition of terms used within the DDC pages. `http://www.ipcc-data.org/guidelines/pages/definitions.html`, 2013.

[59] Intergovernmental Panel on Climate Change. Scenario Process for AR5. `http://sedac.ipcc-data.org/ddc/ar5\_scenario\_process/scenario\_background.html`, 2014.

[60] M. Pasalodos-Tato, A. MÃďkinen, J. Garcia-Gonzalo, J.G. Borges, T. LÃďmÃěs, and L.O. Eriksson. Review. assessing uncertainty and risk in forest planning and decision support systems: review of classical methods and introduction of new approaches. *Forest Systems*, 22(2), 2013.

[61] Robin C Purshouse and Peter J Fleming. Conflict, harmony, and independence: Relationships in evolutionary multi-criterion optimisation. In *International Conference on Evolutionary Multi-Criterion Optimization*, pages 16–30. Springer, 2003.

[62] Stephanie Rebain and Marc E McDill. A mixed-integer formulation of the minimum patch size problem. *Forest Science*, 49(4):608–618, 2003.

[63] Lester Henry Reineke. Perfecting a stand-density index for even-aged forests. 1933.

[64] Elizabeth Reinhardt and Nicholas L Crookston. The fire and fuels extension to the forest vegetation simulator. 2003.

[65] Jason R Schott. Fault tolerant design using single and multicriteria genetic algorithm optimization. Technical report, DTIC Document, 1995.

[66] Svetlana A (Kushch) Schroder, Sándor F Tóth, Robert L Deal, and Ettl Gregory J. Multi-objective optimization to evaluate tradeoffs among forest ecosystem services following fire hazard reduction in the Deschutes National Forest, USA. *Ecosystem Services*, Special Issue "Integrated Valuation of Ecosystem Services: Challenges and Solutions", accepted.

[67] Svetlana Kushch Schroder. *Optimizing forest management in consideration of environmental regulations, economic constraints, and ecosystem services.* PhD thesis, 2013.

[68] Rupert Seidl, Werner Rammer, Dietmar Jäger, and Manfred J Lexer. Impact of bark beetle (< i> ips typographus</i> l.) disturbance on timber production and carbon sequestration in different management strategies under climate change. *Forest Ecology and Management*, 256(3):209–220, 2008.

[69] José Oscar H Sendín, Antonio A Alonso, and Julio R Banga. Efficient and robust multi-objective optimization of food processing: A novel approach with application to thermal sterilization. *Journal of Food Engineering*, 98(3):317–324, 2010.

[70] Daniel Simberloff. Flagships, umbrellas, and keystones: is single-species management passé in the landscape era? *Biological conservation*, 83(3):247–257, 1998.

[71] Soil Survey Staff. Soil survey geographic (ssurgo) database.

[72] Chris D Thomas, Alison Cameron, Rhys E Green, Michel Bakkenes, Linda J Beaumont, Yvonne C Collingham, Barend FN Erasmus, Marinez Ferreira De Siqueira, Alan Grainger, Lee Hannah, et al. Extinction risk from climate change. *Nature*, 427(6970):145–148, 2004.

[73] Sándor Tóth. *Modeling Timber and Non-timber Trade-offs in Spatially-Explicit Forest Planning*. PhD thesis.

[74] Sándor Tóth and Marc McDill. Finding efficient harvest schedules under three conflicting objectives. 2009.

[75] Sándor Tóth, Marc McDill, and Stephanie Rebain. Finding the efficient frontier of a bi-criteria, spatially explicit, harvest scheduling problem. 2006.

[76] Sándor F Tóth, Gregory J Ettl, Nóra Könnyű, Sergey S Rabotyagov, Luke W Rogers, and Jeffrey M Comnick. Ecosel: multi-objective optimization to sell forest ecosystem services. *Forest Policy and Economics*, 35:73–82, 2013.

[77] Sándor F Tóth and Marc E McDill. Finding efficient harvest schedules under three conflicting objectives. *Forest Science*, 55(2):117–131, 2009.

[78] Fernando Badilla Veliz, Jean-Paul Watson, Andres Weintraub, Roger J-B Wets, and David L Woodruff. Stochastic optimization models in forest planning: a progressive hedging solution approach. *Annals of Operations Research*, pages 1–16, 2014.

[79] James M Vose, David Lawrence Peterson, Toral Patel-Weynand, et al. *Effects of climatic variability and change on forest ecosystems: a comprehensive science synthesis for the US forest sector*. US Department of Agriculture, Forest Service, Pacific Northwest Research Station Portland, OR, 2012.

[80] Yu Wang, Hailian Yin, Shuai Zhang, and Xiongqing Yu. Multi-objective optimization of aircraft design for emission and cost reductions. *Chinese Journal of Aeronautics*, 27(1):52–58, 2014.

[81] Lyndon While, Philip Hingston, Luigi Barone, and Simon Huband. A faster algorithm for calculating hypervolume. *IEEE transactions on evolutionary computation*, 10(1):29–38, 2006.

[82] Andy White and Alejandra Martin. Who owns the worldâĂŹs forests. *Forest Trends, Washington, DC*, 2002.

[83] Steven M Wondzell and John G King. Postfire erosional processes in the pacific northwest and rocky mountain regions. *Forest Ecology and Management*, 178(1):75–87, 2003.

[84] Rasoul Yousefpour, Jette Bredahl Jacobsen, Bo Jellesmark Thorsen, Henrik Meilby, Marc Hanewinkel, and Karoline Oehler. A review of decision-making approaches to handle uncertainty and risk in adaptive forest management under climate change. *Annals of forest science*, 69(1):1–15, 2012.

[85] Eckart Zitzler. *Evolutionary algorithms for multiobjective optimization: Methods and applications*, volume 63. Citeseer, 1999.

[86] Eckart Zitzler, Lothar Thiele, Marco Laumanns, Carlos M Fonseca, and Viviane Grunert Da Fonseca. Performance assessment of multiobjective optimizers: an analysis and review. *Evolutionary Computation, IEEE Transactions on*, 7(2):117–132, 2003.

Appendix A

TREATMENT SPECIFICATIONS FOR THE DRINK AREA

Table A.1 provides a mapping from a stand's vegetation conditions to the treatment action to apply to the stand. If a stand's conditions do not correspond to any row in the table, then no action is taken. The table was adapted from Schroder [66]. The plant association groups in the Drink area are shown in Figure A.1.

Table A.1: Rules governing treatment assignments.

SDI[1]	**CBD**[2]	**TPH**$_{<18}$[3]	**Fuel model**[4]	**BA**$_{\text{MHD+WF},>46}$[5]	**Treatment**
Lodgepole pine (LPD) plant association					
< 87	N/A	N/A	N/A	N/A	**Prescribed burn**
≥ 87	> 0.037	> 49	≥ 10	N/A	**Thin, pileburn slash and fuels**[6]
			< 10	N/A	**Thin, pileburn slash**
Mixed conifer wet (MCW) or mountain hemlock (MHD) plant associations					
< 87	N/A	N/A	N/A	N/A	**Prescribed burn**

[1]Stand Density Index, calculated in metric units (trees per ha).

[2]Crown bulk density (kg/m^3)

[3]Number of trees per hectare whose diameter at breast height (DBH) is less than 18 cm

[4]According to the Anderson rating system[4]

[5]Basal area in m^2 of all mountain hemlock (MHD) and white fir (WF) trees with DBH $> 46cm$.

[6]Pileburning slash involves removal of thinned trees only, while pileburning slash and fuels also involves removal of materials that were on the ground before thinning (Wall, Powers, 2012; personal communication)

≥ 87	> 0.037	> 49	$= 10$	> 7.5	**Thin, pileburn slash and fuels, prescribed burn**
				≤ 7.5	**Thin, pileburn slash and fuels**
			> 10	N/A	**Thin, pileburn slash and fuels**
			< 10	N/A	**Thin, pileburn slash**
		≤ 49	$= 10$	≥ 7.5	**Prescribed burn**
	≤ 0.037	N/A	$= 10$	≥ 7.5	**Prescribed burn**
	N/A	N/A	$\in \{6, 8, 9, 10\}$	N/A	**Prescribed burn**[7]
Mixed conifer dry (MCD) plant association					
< 87	N/A	N/A	N/A	N/A	**Prescribed burn**
≥ 87	> 0.037	> 49	$\in \{10, 11\}$	N/A	**Thin, pileburn slash and fuels, prescribed burn**
			≥ 12	N/A	**Thin, pileburn slash and fuels**
			< 10	N/A	**Thin, pileburn slash**
		≤ 49	$\in \{10, 11\}$	N/A	**Prescribed burn**
	≤ 0.037	N/A	$\in \{10, 11\}$	N/A	**Prescribed burn**
	N/A	N/A	$\in \{6, 8, 9, 10\}$	N/A	**Prescribed burn**[7]

[7] Only if prescribed burn was assigned in period 1 (applies to period 2 treatment assignments only)

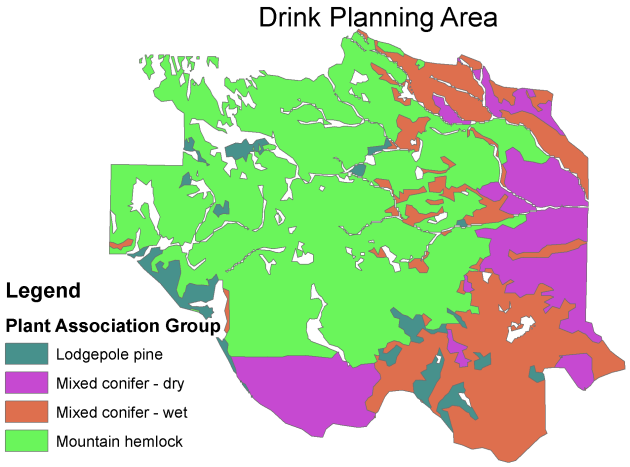

Figure A.1: Plant association groups in the Drink Area that are considered for treatments.